ADDIS ABABA UNIVERSITY
ADDIS ABABA INSTITUTE OF TECHNOLOGY
CENTER OF ENERGY TECHNOLOGY

Performance Simulation of Solar Adsorption Cooler with Activated Carbon-R134a pairs (ACF-A20, Granular AC and Maxsorb III)

A Thesis Submitted to Center of Energy Technology in Partial Fulfillment of the Requirements for the Degree of Master of Science in Energy Technology

Advisor – Solomon T/Mariam (PhD.)

By - Samuel Teka Zewdie

June, 2020

Addis Ababa, Ethiopia

DECLARATION

The undersigned declare that the thesis entitled '**Performance Simulation of Solar Adsorption Cooler with Activated Carbon-R134a pairs (ACF-A20, Granular AC and Maxsorb III)**' is an original research paper prepared and presented by **Samuel Teka Zewdie** under the supervision of Dr. Solomon T/Mariam It has not been presented as a thesis in any other university & all source material used for this thesis are duly acknowledged.

Samuel Teka Zewdie _____ _____

Date Signature of Student

This is to certify that the above declaration made by the candidate is correct to the best of my knowledge.

Solomon T/Mariam (PhD.) _____ _____

Date Signature

UNDERTAKING

I certify that the research work titled '**Performance Simulation of Solar Adsorption Cooler with Activated Carbon-R134a pairs**' is my own work. The work has not been presented elsewhere for assessment. Where material has been used from other sources it has been properly acknowledged / referred.

Name of Student - Samuel Teka Zewdie

Signature of Student - _____

Date : - _____

Addis Ababa University

Addis Ababa institute of Technology

Center of Energy Technology

Performance Simulation of Solar Adsorption Cooler with Activated Carbon-R134a pairs (ACF-A20, Granular AC and Maxsorb III)

By: Samuel Teka Zewdie

Approved by Board of Examiners:

(Advisor)	Signature	Date
(Internal Examiner)	Signature	Date
(External Examiner)	Signature	Date
(Chairman)	Signature	Date
(Director of graduate Programs)	Signature	Date

Abstract

Solar thermal energy can be used to drive sorption coolers. Some of the sorption cooling systems are absorption, adsorption and desiccant systems. This research paper focuses on the performance analysis of adsorption refrigeration system that utilizes activated carbon-R134a pairs. To this end, three variants of activated carbon were assessed for their performance. These types of activated carbon are: ACA-F20, Granular activated carbon and Maxsorb III. These adsorbent materials have varying pore diameter, surface property and adsorption capacities.

The solar adsorption system is highly dependent on pressure, temperature and concentration of the adsorbate on the surface of the adsorbent material. Based on the pore diameter of activated carbon Dubinin-Astakhov equation was selected to characterize the adsorption pairs and simulate using MATLAB. For the Dubinin-Astakhov equation, values of characteristic energy, maximum adsorption capacity and exponential constant were adopted from the works of other researchers: Loh and Askalany.

The coefficient of performance values of ACA-F20-R134a, Granular-R134a and Maxsorb III-R134a were found to be 0.27, 0.2908 and 0.311 respectively at bed temperature of 280K. The specific cooling power values for these pairs were 39.29, 49.03 and 62.09 W/kg respectively.

Some researchers proposed complex system and found performance values with coefficient of performance values ranging between 0.38-0.7. In this specific research lower values were attained using solar energy unlike the other research works that focused on performance analysis of activated carbon and R134a using waste heat and two stage processes that tend to give higher the cooling effect obtainable by refrigerant R134a. As a result the coefficient of performance values were higher than the one obtained in this research.

Keywords: Adsorption refrigeration, Activated Carbon, R134a, Coefficient of Performance, Specific cooling power, Dubnin Asthakov equation

Acknowledgement

First and Foremost I would like to thank God for helping me get through the laborious task of finishing my Msc thesis. I would also like to thank my Advisor Dr. Solomon T/Mariam for his unwavering support throughout this process. His comments and constructive critique were instrumental in the realization of this thesis work.

My gratitude also goes out to Mr. Hintsa and Mr. Feysal who guided me through the laboratory preparation of activated carbon and testing procedures. I also thank Mr. Addis and Mr. Masresha who contributed a lot in the construction of adsorption refrigerator prototype.

Last but not least, I would also like to thank my friends and my family who have played pivotal role in the realization of this thesis work.

Table of Contents

List of Figures

List of Tables

Chapter 1
Introduction

1.1 Background

Refrigeration is a process of transporting heat from a place of lower heat to a higher heat source through heat pumps. Hence, this process plays a vital role in the daily livelihoods of millions of people in areas of food preservation, pharmaceutical industry and other sectors. However, as more and more heat pumps are being employed the concern on their energy utilization (especially during peak seasons) and usage has become a topic of research interest.

Energy utilization for cooling systems is one of today's concerns since most of such systems are vapor compression cooling systems which use electricity. Energy supply to refrigeration and air conditioning systems constitutes a significant percentage of energy consumption in our world. The International Institute of Refrigeration (IIR) estimates that approximately 15% of all electricity produced worldwide is used for refrigeration and air conditioning processes of various kinds (Lucas, 1988). Currently, there are many researchers who focus on alternative technologies to run the cooling systems efficiently by renewable energy sources like solar energy.

One of these technologies is solar adsorption refrigeration technology. Since late 1970's rigorous research has been carried out to assess the viability and commercial potential of solar sorption refrigeration system (Wang, Oliveira, 2006). The main sorption refrigeration cycles are dessicant, absorption and adsoption refrigeration cycles.

An Absorption refrigeration cycle uses liquid substance able to absorb another liquid substance that acts as the refrigerant. The absorbent has the ability to absorb large quantities of vapor when cold and gives it up when heated. The main components of the system are an absorber, a generator, a condenser an expansion valve, an evaporator, a heat exchanger and pump.

A desiccant cooling system combines dehumidification and evaporative cooling processes. In this system, outdoor air is dehumidified with a solid or liquid desiccant where some of the moisture is removed, resulting in rising of the air temperature and decreasing of the humidity. The air is then cooled by exchanging sensible heat to the returned air in the heat exchanger. The temperature of

the supply air is further lowered and humidified to the desired humidity by the humidifier or the evaporative cooler before entering the cooling space. The returned air from the cooling space is returned to the evaporative humidifier.

Solar adsorption refrigeration uses different adsorbate-adsorbent pairs such as zeolite-water, silica gel-water, activated carbon-methanol and various chemical and composite type pairs to yield refrigeration effect. This technology uses environment friendly refrigerants such as water, ammonia and methanol which have zero ozone depletion potential and null global warming potential. To a certain extent, these systems have been successful in various areas of the world.

However, studies on efficiency of activated carbon-R134a pairs are few and comparative studies of different types of activated carbon and R134a pairs have not been extensively researched. Hence, this serves as the research gap identified in this paper and a topic of study. This study therefore compares the performance of three varieties of activated carbon against R134a refrigerant and studies the economic viability of the best choice.

The use of adsorption refrigeration is more pronounced in countries that have abundant solar energy source like Ethiopia. As a country located around the equator, Ethiopia is endowed with sufficient solar energy which helps it promote and cultivate the technology until commercial electricity is disseminated throughout much of its remote areas. Therefore, studying the performance of adsorption pairs for refrigeration applications is of great value.

1.2 Statement of the Problem

In tropical regions like Ethiopia, perishable foods such as products of the fishery and cattle farming sectors are commonly wasted due to lack of proper preservation methods. Additionally, securing chilled water is not easily achievable since conventional refrigeration systems are mostly electrically powered. This shortcoming is also associated with the fact that thermal driven refrigeration systems are still under research and not commercially available.

Particularly, when it comes to the study of adsorption refrigeration only few studies have been conducted and rudimentary stages of development have been assessed in this research area. There might be several reasons for insufficient study of this technology. Some of them are high

efficiency of refrigeration by electric powered vapor compression system, wide acceptance of vapor compression systems and lack of effort to boldly commercialize adsorption refrigeration technology.

At the end of this paper work, the following questions related to adsorption technology will be answered:-

1. What are the performance assessment parameters of adsorption refrigeration technology?
2. What are the characteristics of the basic adsorption refrigeration systems analyzed?
3. Of the different adsorbate-adsorbent pairs, which one is the most effective and efficient for the purpose of adsorption refrigeration?

1.3 General Objective

The main objective of this study is to simulate a solar adsorption refrigeration system for conservation of perishable foods and preparation of chilled water.

1.3.1 Specific Objectives

This study on adsorption refrigeration has the following specific objectives which are integral part to the main aim of the thesis work.

1. Determining the performance effect of different types of activated carbon paired with R134a refrigerants and select the best adsorbent/refrigerant pair
2. Simulation and optimization of the adsorption refrigeration system
3. Validation of the study based on other researches.

1.4 Scope of the Research

This paper focuses on performance simulation of adsorption cooler system that utilizes Activated-Carbon-R-134a as adsorption pairs. In this paper, three types of commercial activated carbon were considered. These adsorption pairs are physical adsorption systems by nature which means that this paper does not delve deep into other types of adsorption pairs namely; chemical, composite and novel adsorption pairs. The performance of the adsorption pair was analyzed using MATLAB simulation tool and the coefficient of performance (COP) and specific cooling power (SCP) were analyzed and the comparative advantages of using the three adsorption pairs is discussed in detail.

1.5 Significance of the Study

Conducting this research is important to our country since it enables to exploit the riches of Ethiopia's solar energy potential. Apart from that, Ethiopia can reduce its annual energy consumption of electricity if this technology can successfully be applied to the manufacturing and agricultural sectors. With these visions in sight in the long run, working on the analysis of the adsorption refrigeration technology can lay down basic building blocks towards the development and growth of this technology. Some beneficiaries of the technology are rural communities engaged in fishery, cattle herding and refugees located in the different part of Ethiopia.

Chapter 2
Literature Review

2.1 Adsorption Phenomena

Adsorption, also referred to as solid sorption is a technique that is usually employed to attract liquid or vapor substances, termed as adsorbate, on to the surface of an adsorbent. The process operates based on temperature and pressure gradient on the adsorbent where higher temperature with respect to the environment regenerates the adsorbate and lower temperature gradient enables it to adsorb.

The type of adsorbent/adsorbate pairs has a great effect on the performance and characteristics of the system. Most commonly, there are three types of physical working pairs that are considered to deliver the best results for solar cooling technology (Mahmoud et al., 2018). These systems are silica gel/water, zeolite/water and Activated Carbon/(HCFC/Ammonia/Methanol) pairs.

The simple adsorption refrigeration cycle has four basic processes. Two of them are isosteric heating and cooling processes while the other two are isobaric adsorption and desorption processes. The clapeyron diagram for the thermodynamic cycle is shown in Figure 2.1.

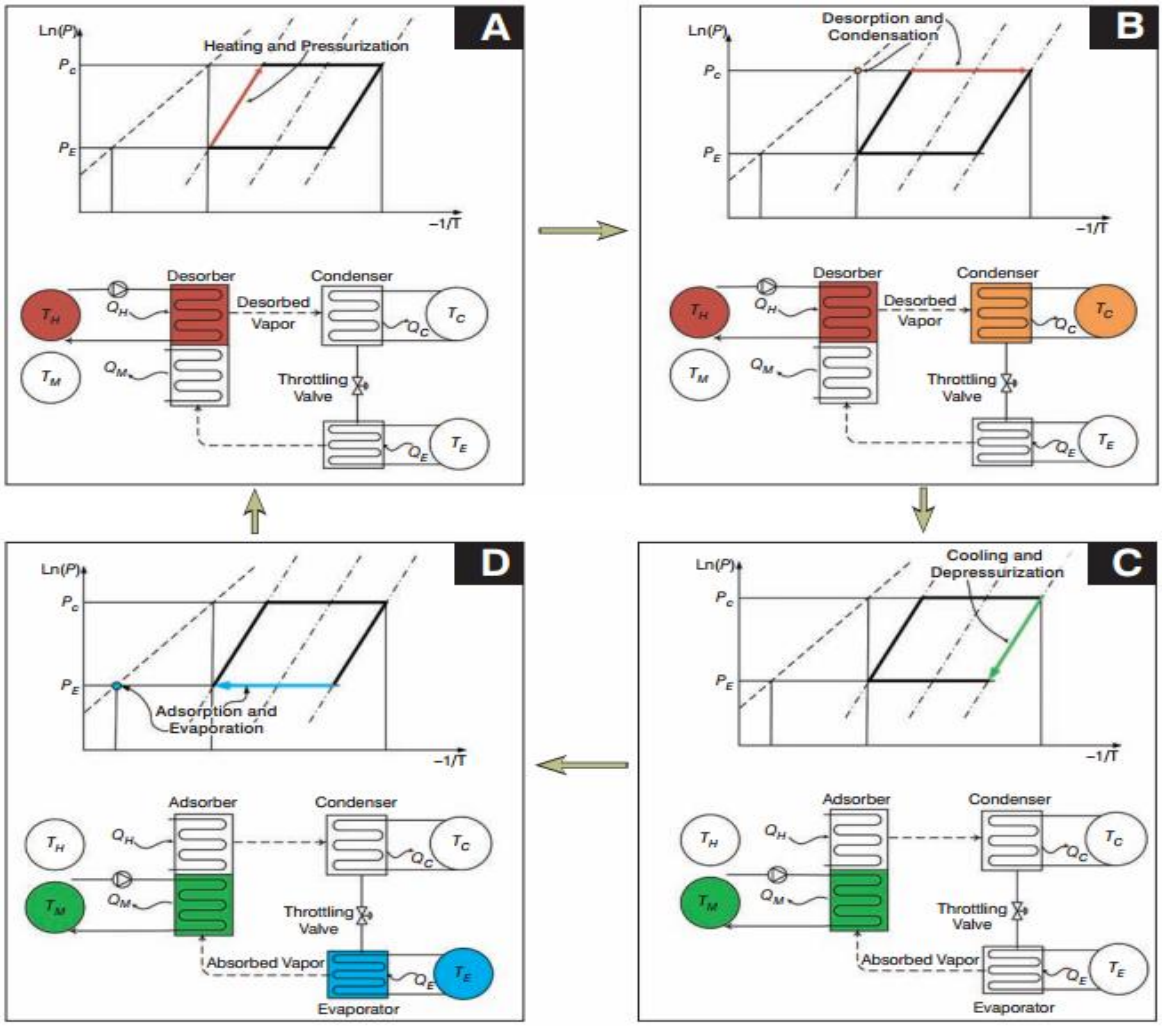

Figure 1.1 - Basic adsorption refrigeration system. ***A.*** *Heating and pressurization.* ***B.*** *Desorption and condensation.* ***C.*** *Cooling and depressurization.* ***D.*** *Adsorption and evaporation.* ***(****Kai Wang et al., 2011****)***

The four cycles of the refrigeration process can be described as follows.

Pre-heating process (A): In this heating and pressurization period, the valves between the adsorbent bed and both of the condenser and the evaporator are closed, and the adsorbent bed is operated as a closed system that is subjected to heat source at temperature T_H. Meanwhile, the bed temperature increases sensibly which induces the vapor pressure inside the bed to increase as well. This process lasts until the vapor pressure rises from evaporator pressure P_e to P_c.

Generation process (B): Once the condenser pressure is reached, further heating should take place by opening valve in the bed and condenser. The bed temperature is continuously increased till the design temperature. This is the phase where desorption of the refrigerant takes place.

Pre-Cooling process (C): After the bed reaches the maximum temperature at desorption temperature, the cooling and depressurization of the bed takes place. The temperature from this point on is decreased gradually as it goes from P_c to P_e. Hence, the pressure inside the adsorber bed is reduced to the evaporator pressure level by the end of this process.

Adsorption process (D): In this process, the valve between the adsorber and the evaporator is opened, and the adsorber is continuously subjected to cooling. Then, the vaporized refrigerant in the evaporator, which gives the cooling effect, is directed to the adsorber bed.

2.2 Review of related literature

Increasing price of conventional fossil fuel and the associated environmental impact have forced the world to look into other sources of energy. The alternative technologies had to be sustainable, available at low cost and free of pollution. One of the alternative energy options is solar energy which is instrumental for different applications such as refrigeration and air conditioning. For remote and inaccessible areas, adsorption refrigeration is a thermal driven refrigeration system which can be powered by solar energy as well as waste heat.

An advantage of adsorption refrigeration systems compared with conventional vapor compression systems is the working fluid used. In contrary to HCFC and CFC as refrigerants, it uses innocuous and environmentally friendly refrigerants. Adsorption systems mainly use a natural working fluid such as water and ammonia, which have zero ozone depletion potential (Dusane and Ghuge, 2016).

The need to conserve energy and the fact that adsorption refrigeration systems can be activated using low grade heat source has led the scientific community to pursue study in adsorption refrigeration systems. Solar adsorption refrigeration systems have additional advantages other than low ozone depletion potential and low grade heat utilization. One of these advantages is operating over a wide range of temperature. Adsorption systems can be activated by heat sources as low as

50°C, and the heat source temperature for an absorption system should be at least 90°C (Wang et al., 2009). Hence, solar flat plate collectors can easily be used. Also, adsorption systems have less corrosion issues for the adsorbent-refrigerant working pairs.

Another advantage is their suitability for application where serious vibration occurs (Wang, et al., 2008)**.** In other refrigeration systems such as absorption refrigerators, used for fishing boats and locomotives, the absorbent liquid solution may flow from the generator to the condenser in cases where there is a serious vibration in the system. Adsorption systems are suitable for such applications, because their adsorbents are stable and can be used as portable cooling system.

Based on the nature of attractive forces between adsorbent-adsorbate materials, adsorption phenomena can be grouped as physical adsorption or chemical adsorption. In physical adsorption, the dominant forces of attraction are weak Van der Waals' type. Due to its weakness, physical adsorption can be easily reversed by heating.

In chemical adsorption, the forces of attraction and chemical bonds between the adsorbate and adsorbent molecules are strong. The adsorbate and adsorbent molecules change their original state after the adsorption process, e.g., complexation occurs between chlorides and ammonia. The chemical bonds also show a phenomena of salt swelling or agglomeration which heavily affects the heat and mass transfer performance of the refrigeration system (Wang et al., 2009). The major drawbacks of adsorption systems are their low energy efficiency which is expressed by their low COP (coefficient of performance: the ratio of cooling capacity to amount of work supplied to the system) which is usually less than 0.4. This is majorly due to the thermal coupling irreversibility (Meunier et al., 1996).

2.3 Adsorption Working Pairs

The performance and operating parameters of adsorption refrigeration systems are affected by the choice and characteristics of the adsorbent/refrigerant working pairs. Good adsorbents possess wider range of adsorption capacity with temperature variation, higher heat and mass transfer properties, along with thermal stability and low susceptibility to contamination. Other properties of the working pairs such as heat of vaporization, thermal conductivity, boiling point and working pressures, reactivity and stability, toxicity, environmental impact and freezing point are also of

interest in the selection process. Adsorption capacity of adsorbent-refrigerant pair is commonly determined from plots known as adsorption isotherms (Elsheniti et al., 2018). An example of such curve is given with silica-gel-water pairs shown in figure 2.2 (Zimmermann et al., 2004).

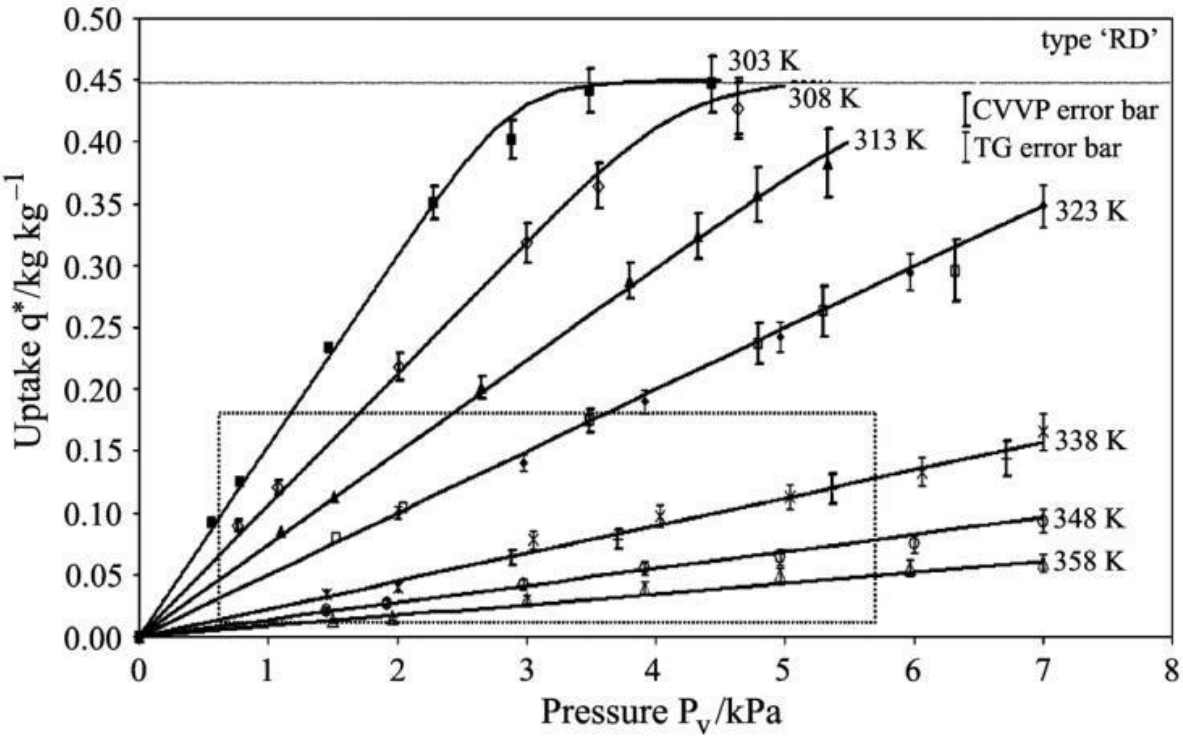

Figure 2.2 - Isotherm data for type 'RD' silica gel-water system fitted using Toth's equation (Zimmerman et al., 2004)

These isotherms give the amount of adsorbed mass taken up by the adsorbent as a function of pressure at constant temperatures. From the above figure we can see that maximum adsorption capacity/uptake of 0.45 kg adsorbate/kg of adsorbent can be obtained at 303K for 'RD' Silica gel-water systems under the Toth correlation. Hence, the kinetic model defines the mass transfer rate and gives the instantaneous amount of adsorbate through a relation with the equilibrium uptake that is given by the isotherms.

Mass transfer kinetics defines the system's resistance to the mass transfer making it an important parameter when selecting the right type of working pairs. Increment in the adsorption capacity increases the cooling capacity and the refrigerant amount that can be adsorbed in a cycle. However, faster mass transfer kinetics is required to ensure higher cooling capacity.

2.3.1 Physical adsorbent-adsorbate pairs

The physical adsorbents are adsorbent complexes which rely on van der waals forces to adsorb the refrigerant adsorbate. The most common physical adsorbent-adsorbate pairs are discussed as follows.

2.3.1.1 Silica gel-water systems

Silica gel is a form of silicon dioxide, produced synthetically from sodium silicate having granular and porous form. Most commonly used silica-gel types are Fuji Davison type A and RD selected specifically for their high density and small pore volume and diameter. Their pore diameter is in the range of 2.0-3.5 nm, the pore volume is 0.3–0.4 cm^3/g and the specific surface area is 400–700 m^2/g (Aristov, 2007).

Generally, silica gel is more advantageous in areas of application where the required regeneration temperature is typically 85°C. This makes it particularly suitable for solar and low grade energy resource utilization applications. More suitably, the regeneration temperature can even drop to 50°C when multi-stage cooling is applied (Saha et al., 2001). However, if desorption temperature is higher than 120°C, silica gel will be destroyed. The adsorption heat is between 2500 and 2800 kJ/kg which is relatively higher than activated carbon.

However, silica gel has a porosity level of 100–1000 m^3/g which is lower than activated carbon and inhibits it from adsorbing more amount of refrigerant. The maximum adsorption capacity at equilibrium could be between 0.35 and 0.4 kg/kg silica gel. Another shortcoming is the limitation of evaporating temperature due to the freezing point of water and the uptake also is affected badly under a very low vacuum, that make silica gel-water refrigeration system be better applied in the air conditioning applications. The COP of silica gel-water adsorption refrigeration systems ranges from 0.3-0.6 (Wang and Oliveira, 2006).

2.3.1.2 Zeolite-water systems

Zeolites are microporous crystals that constitute alkali soil. The zeolite-water working pair has a wide range of desorption temperature (70–250°C). This particular trait had enabled this working pair to be stable at high temperatures and it can be heated directly from gases from

engines. However, it requires higher heat of adsorption which is usually in the range of 3300 to 4200 kJ/kg (Kai and Wang, 2011) which leads to low COPs.

2.3.1.3 Activated carbon (HCFC/ammonia/methanol) systems

Activated carbon is a form of carbon that has a large specific area available for adsorption between 800 and 1500 m^2/g for most used carbon. Activated carbon has advantages of relatively low adsorption heat among the other types of physical adsorbent pairs (1800–2000 kJ/kg) (Kai and Wang, 2011). Low adsorption heat is beneficial to the system's COP because the majority of heat consumption in the regeneration phase is the adsorption heat, higher surface reactivity, suitable pore size and large surface area. Despite these shortcomings, these systems have higher COP values as compared to other physical adsorbents owing to the fact that they adsorb high amounts of adsorbates.

2.3.2 Chemical adsorbents-adsorbate pair

Chemical adsorbents adsorb refrigerants differently than physical adsorbents. The strong chemical bond between the adsorbent and the refrigerant governs the bonding in chemical adsorption. The fact that the uptake is not limited by the surface area of the adsorbent gives rise to higher mass transfer kinetics when compared to physical adsorbents. Metal chlorides are commonly used as chemical adsorbents due to their high adsorption capacity, and they involve calcium chloride ($CaCl_2$), strontium chloride ($SrCl_2$), magnesium chloride ($MgCl_2$) among others. As an example, in $CaCl_2$/ammonia pair, 1 mole calcium chloride can adsorb 8 moles ammonia. **(**Wang et al., 2010**)**. However, the problem of agglomeration or swelling exists when using metal chlorides as adsorbents which is a drawback in chemical adsorption pairs.

2.3.3. Composite adsorbent-adsorbate pairs

Composite adsorbents, also called Salt in Porous Matrix (CSPM), are hybrid working pair aimed at solving the drawbacks associated with pure physical and chemical adsorbents. Thus, many of these composites have been developed synthetically to be applied in adsorption refrigeration systems (Gordeeva, et al., 2013). In such composites, the porous media work on improving the heat and mass transfer properties of the chemical adsorbents along with limiting the swelling

characteristics of the chemical adsorbents. Hence, this creates a composite material having the advantageous characteristics of the individual chemical and physical adsorbent materials.

Composite pairs are usually combinations of activated carbon, silica gel or zeolite with metal chlorides. These pairs are usually manufactured by impregnation method where the physical adsorbent is immersed in chloride salt and dried to remove the water. This creates a unique adsorbent having properties of both the metal chloride salt and the physical adsorbent.

2.3.4 Novel adsorbent materials: metal-organic frameworks (MOFs)

Metal-organic frameworks (MOFs) are highly crystalline porous materials widely regarded as promising materials for various applications such as catalysis, gas separation and gas storage. MOFs are designed based on the assembly of organic units and metal clusters as secondary building units to build the robust complex structures. When compared to conventional material such as silica gel and zeolites, MOFs were found to be flexible in controlling their architecture and functionalization of the pores (Li, et al., 1999). Such manageable properties have given the lead to MOFs over conventional adsorbents as they offer high stability and porosity. As such, the superior qualities of these novel adsorbent materials have made them very suitable and interesting for various applications.

2.4 Properties of adsorbents and adsorbates

Any adsorbent-adsorbate working pair should possess certain types of traits that are ideal to its efficient working. Below is the desired properties of both adsorbates and adsorbents used in adsorption refrigeration and heat pumping.

2.4.1 Desirable properties of adsorbate

The properties of ideal adsorbate used in solar adsorption system are as follows (Salem, 2010):

- Evaporation temperature below 0°C (for refrigeration purposes it can be higher in the case of air-conditioning applications).
- Small molecular size so as to facilitate the adsorption effect
- High latent heat of vaporization and low specific volume when in the liquid state.

- High thermal conductivity.
- Thermally stable with the adsorbent in the operating temperature range.
- Chemically stable in the operating temperature range.
- Low saturation pressures (slightly above atmospheric pressure) at normal operating temperature.

2.4.2 Desirable Properties of adsorbent

The properties of ideal adsorbent used in solar adsorption system are as follows (Salem, 2010):

- Ability to adsorb a large amount of adsorbate when cooled to ambient temperature, to yield a high cooling effect.
- Desorption of most (ideally all) of the adsorbate when heated by the available heat source.
- Low specific heat.
- Good thermal conductivity, to shorten the cycle time.
- Non deterioration and adsorption capacity losses over time or with usage.
- Non-toxic and non-corrosive.
- Chemically and physically compatible with the chosen refrigerant.

2.5 Working mechanisms and thermodynamic properties of physical adsorption

Physical adsorbers have cylindrical porous structures that enable them to operate using the principle of capillary condensation process. Basically, there are three classes of porous medium namely; macropore, mesopore, and micropore. The first class of porous particles, Macropores, are incapable of adsorption due to their large size. The latter two in contrast have adsorption capacity and potential. Microporous structures even possess a higher affinity to adsorbate materials since the saturation pressure required by them is significantly lesser than mesoporous and microporous structures.

2.5.1 Adsorption equations

For physical adsorption, there are three kinds of adsorption equations.

1. **Adsorption rate equations**: - Rate correlations are Langmuir equations applied for monolayer adsorption systems. But since adsorption systems are not monolayer and these equations are not accurate they are no longer used in analysis and evaluation of adsorption systems.
2. **Thermodynamic equations for adsorption processes**: - These equations are based upon polanyi's adsorption potential theory and adsorption theory in micopores proposed by Dubnin. They accurately represent adsorption equilibrium process especially for adsorbate vapor and activated carbon.
3. **Equations for condensation processes of adsorbate vapor in microspores**: - It generally ignores the impact of the energy distribution on the surface of adsorbents. The pores of the adsorbent are considered as capillary pores.

Adsorption potential theory describes the various fields of adsorption potential on an adsorbent. It studies the properties of adsorbate-adsorption potential from the view point of thermodynamics and change of surface gibbs functions. According to this theory, an adsorbent is consisted of different surfaces having varying levels of adsorption potential. There is a point of highest adsorption potential where the adsorption capacity is the largest. As the adsorbate vapor deviates from this center of highest potential, adsorption capacity decreases until a point of zero potential is reached. The adsorption potential as a function of isothermal compression work of the adsorbate is given as follows:

$$\varepsilon = RTln\left(\frac{P_s}{P}\right) \qquad \text{(eq. 2.1)}$$

Where P_s is the saturation pressure corresponding to the adsorption temperature and P is the adsorption pressure at equilibrium condition which is read at saturation pressure. When the adsorption properties of the adsorbent are the same regardless of the adsorbate used the following formula is used.

$$\varepsilon_l = \frac{\varepsilon}{\beta} \qquad \text{(eq. 2.2)}$$

The Dubinin-Radushkevich theory states that the adsorption potential of activated carbon that is made of micropores with radius of 1.8-2 nm follows the Gaussian distribution. Therefore,

the volume of refrigerant V_c adsorbed, the pore volume of adsorbate V_o and the adsorption potential are related as follows.

$$V_c = V_o \exp[-B\left(\frac{\varepsilon}{\beta}\right)^2] \quad \text{(eq. 2.3)}$$

Substituting (2.1) in (2.3) gives:

$$V_c = V_o \exp[-B\left(\frac{RT}{\beta} ln \frac{P_s}{P}\right)^2] \quad \text{(eq. 2.4)}$$

When the adsorption quantity is constant and the temperature change range is small, the relationship between saturation pressure and temperature is expressed by the Clausius-Clapeyron equation which is of the following form:

$$\ln P = A - \frac{C}{T_{sat}} \quad \text{(eq. 2.5)}$$

Substitution of P of (2.5) in P of (2.4) gives:

$$\mathrm{Vc(T, Tsat)} = \mathrm{Vo(Tsat)} \exp\left\{-B\left[\frac{RC}{\beta}\left(\frac{T}{T_{sat}} - 1\right)\right]^2\right\} \quad \text{(eq. 2.6)}$$

Isobaric and isothermal adsorption equations are used widely for the design and simulation of adsorption systems. In a similar manner, D-A and D-R equations are also isobaric equations used for the analysis of micropore adsorption process. These equations are simple and suitable for a wide range of temperature and pressure if the adsorbent has a porous surface or its pore diameters are uniform.

D-A equations are of the following form.

$$X = X_o exp\left(-\left(\frac{\varepsilon}{E}\right)^n\right) \quad \text{(eq. 2.7)}$$

This form of the equation is only used for adsorbents having smooth surface and when the adsorbent employed is weak in polarization.

2.5.2 Adsorption and Desorption Heat

When physical adsorption occurs on the surface of an adsorbent a decrease in the entropy of the vapor occurs as it changes from a more dispersed state to a more ordered one. Hence, by the 2nd law of thermodynamics the free energy is as follows:

$$G = H - T \quad \text{(eq.2.9)}$$

And for a Constant pressure and temperature

$$\Delta H = \Delta G + T\Delta S \quad \text{(eq. 2.10)}$$

This enthalpy is referred to as adsorption heat. Adsorption heat is composed of condensation heat of the vapor and surface energy. The first one occurs as a result of the van der waals' forces between the vapor's molecules while the latter one is a result of the decrease in the entropy of adsorbate vapor molecules upon attracting with the surface of the adsorbent surface. The summation of these two energy types gives us the adsorption energy. However, since measurement of surface energy is difficult we use adsorption equation to find the total adsorption heat.

2.6 Adsorption refrigeration cycles

Since its advent, adsorption refrigeration has developed to incorporate different kinds of cycles. The two common cycles are intermittent cycles and continuous cycles. The first of these two uses a single bed while the latter one uses two or more beds operating interchangeably. If an adsorption refrigeration system only has heating and desorbing and cooling and adsorbing processes it is considered as a basic cycle operation. However, if the system has additional efficiency increasing mechanisms it is considered as and advanced cycle system. Advanced cycles give rise to efficient refrigeration systems by incorporating heat and mass recovery mechanisms.

2.6.1 Heat Recovery cycle

Basic cycle adsorption systems have inherent problem that limits their COP values below 0.4 (Meunier, et al., 1996). This is mainly due to the fact that the adsorption bed undergoes periods of heating and cooling where it releases sensible heat and adsorption heat in adsorption phase and absorbs these two heat types back in the desorption phase. As a result, there will be a considerable amount of change in heat and it greatly affects COP of the system.

For single bed refrigeration system, the cooling and heating is carried out by interchangeable process which makes the system to incur sensible heat loss. But for a multi-bed system, this loss can be prevented. The use of heat recovery offers solution to this persistent problem. It is generally operated at the switch time for the adsorption and desorption processes and could recover the sensible heat to improve the efficiency.

The heat recovery concept operates with the use of recoverer. The recoverer is similar in construction to the adsorbent bed and by alternating the heating and cooling processes, thermal energy is stored in the heat recoverer and released depending on requirements. The heat recoverer used in adsorption systems is the adsorbent bed itself. Hence, when used in conjunction with heat recovery system, an adsorption refrigeration system with is called heat regeneration cycle. The typical cycle for the heat regeneration process is proposed by Tchernev as shown in figure 2.3 (Tchernev and Emerson, 1988).

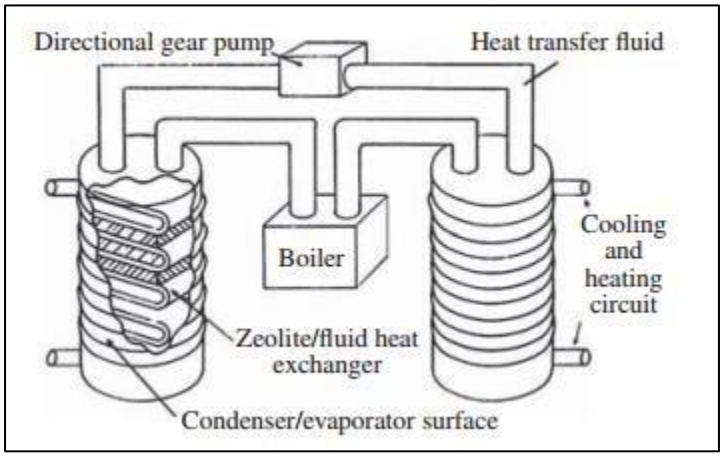

Figure 2.3 - Heat regeneration cycle proposed by Tchernev (Tchernev and Emerson, 1988)

2.6.2 Thermal Wave Cycles

It was Shelton who first proposed using thermal wave in the adsorption system (Shelton, 1990). Compared with the heat recovery process that is limited to only the recovery of the temperature of the beds, thermal wave cycle has a merit of transferring heat from the hot adsorbent bed to cold adsorbent bed due to large temperature gradient.

2.6.2.1 The Principle of the Basic Thermal Wave Cycle

The basic continuous solid adsorption refrigeration system has two adsorbent beds where adsorption and desorption processes proceed alternatively. That is, when one bed is heated by the external heat source for desorption, another bed is cooled by the external cooling source for adsorption. The concept behind the design of a thermal wave cycle is to try to use the exothermic heat Q_a completely and reduce the heat Q_g required by the desorption process from the external heat source. Such process improves the performance of a system significantly.

The basic principle of such a cycle is using a single heating and cooling fluid circuit to connect two adsorbent beds, the cooler, and the heater. Hence, the fluid transfers the released heat of the adsorption bed to desorption bed and recovers heat from adsorption that improves the systems energy efficiency. The efficiency of heat recovery is as high as 80% in this heat regeneration system.

The thermal wave cycle requires that the temperature at the outlet (T_B) of the desorption bed be low, while the temperature at the outlet of the adsorbing bed is relatively high. Otherwise, a big amount of the heat will be released at the cooler, and for such a process it is difficult to recover the heat back to the heater effectively.

2.6.3 Mass Recovery Cycle

The mass recovery cycle is carried out between/among two or more adsorbent beds in the adsorption system at the switch time. The cooled adsorbent bed before switch time is connected with the evaporator, and its pressure is close to the evaporation pressure at the switch time. On the other hand, the hot adsorption bed is connected with the condenser and the pressure is close to condenser pressure. Under this condition, connecting the hot bed with the cold bed at the switch time can greatly increase the desorption rate of the hot bed, which will be helpful for the improvement of the adsorption quantity of the hot bed in the next half cycle for the cooling and adsorption process, and thereby it will improve the cooling capacity.

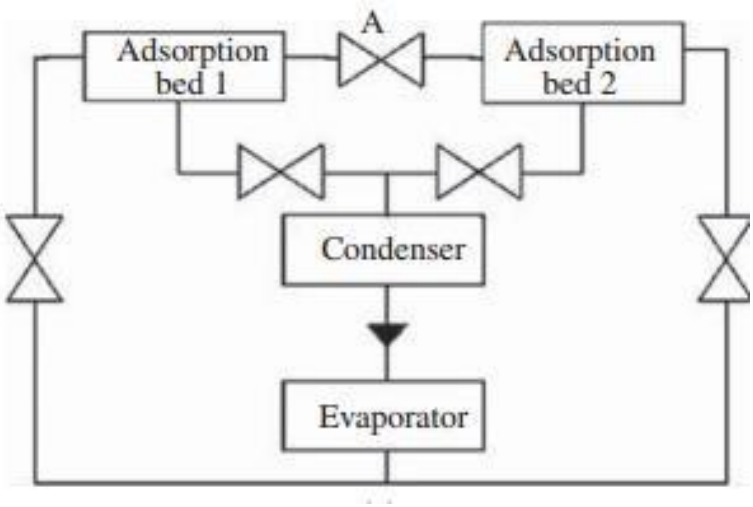

Figure 2.4 - Operating principle of mass recovery cycle (Wang et al., 2014)

A typical mass recovery cycle operates as depicted in figure 2.4. When the desorption of adsorbent bed 1 finishes, the adsorption of bed 2 also finishes. Then the valves connecting the adsorption beds, evaporator, and condenser are closed and valve A is opened for mass recovery between the high-pressure adsorbent bed (hot bed) and low-pressure adsorbent bed (cold bed). As such, the mass recovery will proceed between two beds.

2.7 Current Research trends in Adsorption refrigeration

The current research trends in adsorption refrigeration mainly focus on three areas namely; heat transfer intensification, development of novel adsorbate/adsorbent pairs and utilization of low grade heat and solar energy. The first of these focuses on mechanisms that enhance the heat transfer capacity of adsorption refrigeration systems by different techniques. These techniques include improving the heat transfer by increasing heat transfer area, use of compact adsorption bed, heat pipe technology and implementation of coated heat exchanger.

Another area of research is the utilization of low grade heat and solar energy to make it usable in either remote parts of the world or utilize exhaust heat of different processes and operations to run adsorption refrigerators. Low grade heat from locomotives have been researched extensively to utilize the exhaust from cars and fishing boats for adsorption refrigerators.

Another area of research is the research on novel adsorbate/adsorbent working pairs that are more efficient. This area of research is focused on improving the adsorption capacity of working pairs so that better cooling performance can be obtained. To this end, composite working pairs and MOFs have been developed which can make adsorption refrigeration more competitive and marketable as other types of refrigeration systems.

2.7.1 Heat Transfer Intensifcation Technologies

In order to improve the cooling capacity of an adsorption refrigeration system, the cycle time should be short. We can deduce this from the specific cooling capacity formula which is given approximately as follows.

$$SCP \approx \frac{L\Delta x}{t_c} \qquad \text{(eq. 2.11)}$$

L is the latent heat of vaporization of the refrigerant, t_c is cycle time, and Δx is cycle adsorption quantity. The equation shows that shortening the cycle time gives improved cooling capacity. This can be achieved in two ways. The first one is to improve the mass transfer performance of the system while it is at low pressure working condition and the second one is to enhance the heat transfer performance of the adsorption bed.

The two main technologies known to have enhanced heat transfer are heat transfer intensification technologies for the adsorbent and adsorber. The former one concentrates on the development of the novel types of adsorbents, and the latter one concentrates on the development of the new type of heat exchangers for the adsorber. This has three areas of development which include increasing the heat transfer area of heat exchanger, utilizing a compact adsorption bed or coated adsorber, and the last one is to use heat pipe technology.

2.7.1.1 Heat Transfer Intensification by Extending the Heat Transfer Area

Extended heat transfer equipment provide a good means of improving heat transfer efficiency. Finned tube, plate heat exchanger, and plate-fin heat exchangers are commonly used to improve heat transfer area of an adsorption refrigeration system. However, increasing heat transfer area also increases the heat capacity of the metal materials for adsorbers which in turn necessitates the use of advanced cycles for the recovery of heat among adsorbers.

When applying this technology for granular adsorbents the value of the wall heat transfer coefficient depends on the size of the adsorbent material applied. Hence, small sized adsorbent particles are assumed to be necessary for improvement of the heat transfer coefficient. For example, Miles and Shelton, using small particle size of adsorbent, shortened the cycle time to 5 minutes (Miles and Shelton, 1996).

2.7.1.2 Compact Adsorption Bed

Compact adsorption beds are suited for applications where the bulk sorbent is not used. This technology has long been used with metal hydrides. Another method that is associated with the application of using compact beds is the use of adsorbent materials that are hardened further with binders. This particular method improved the thermal conductivity of activated carbon by 58– 100% (Wang et al., 2003). Implementation of compact adsorber beds has the disadvantage that the mass transfer performance will be influenced in the adsorption bed, especially for vacuum operated refrigerant systems such as water and silica-gel and other pairs.

2.7.1.3 Coated Heat Exchanger

When the COP of an adsorption refrigeration system is not a concern this method is usually applied. Hence, coated adsorbent beds can enhance the thermal conductivity of the adsorber effectively by reducing the contact resistance between the heat transfer surface and the absorbent.

Dunne (1996) utilized zeolite coated on the surface of the metal tube thereby improving the SCP to the level of 1500 W/kg.

This technique has a shortcoming that makes it require a heat recovery process when the heat capacity of the metal is too high. Coated adsorbers can be developed by inserting adsorbent materials into extended natural graphite plates (Pons and Dantzer, 1994). In this method, the contact between heat transfer fluid and the adsorbent is not as close as a coated pipe, but since the diameter of the granular adsorbents is only a few microns, the heat capacity of the adsorbent is greatly improved.

2.7.1.4 Heat Pipe Technology

The use of heat pipe technology is another area of heat transfer intensification method. Meunier (1998) put forward a novel idea for the improvement of the heat transfer performance, in which he worked on the phase change processes such as condensation or evaporation, for heating and cooling the adsorber beds hence obtaining high heat transfer coefficient. The concept of pulse heat pipe was introduced by Vasiliev (2005) in which he used propane as the working medium in the design of the pulse heat pipe, for which the adsorption bed is a tablet-shaped heat pipe made of aluminum, and the width of the heat pipe is only 7 mm (Vasiliev, 2005).

2.7.2 Low Grade Heat Utilization

The existence of low grade heat in vast quantities creates the opportunity to recover it for different applications. Low grade heat has the potential to be used in adsorption refrigeration systems and the heat out of exhaust systems from fishing boats and trucks has been a topic of research in recent studies. Adsorption refrigeration technology is suitable for the recovery of most low grade heat resources by different adsorption working pairs. For example, the silica gel–water working pair can be utilized as a heat source with a low temperature, whereas the zeolite–water system is applicable for a high temperature heat source.

The suitability of adsorption is that it provides stable condition in case of vibratory occasions since it uses solid adsorbent that is impervious to changes in motion. As a result, low grade heat utilization using solid adsorption refrigeration has been carried out extensively in recent years. Suzuki (1993) applied the zeolite–water working pair on an adsorption automobile air conditioner and investigated the performance of the system, and found that the results showed improving heat and mass transfer merits is essential to reduce the cycle time and the weight of the system. Zhu et al. (1992) studied the adsorption refrigeration system used for the fish storage on boats. Saha **(**2006**)** presented a double-stage adsorption refrigeration cycle with four beds driven by a low temperature heat source. The system has shown that when the source temperature is very low i.e. less than 54 °C , the system shows higher efficiency for the double stage cycle as compared to single stage cycle. But for higher temperature heat sources the efficiency showed a marked decrease.

2.7.3 Solar Energy Utilization

Since the time when Tchernev (1985) successfully developed a zeolite-water adsorption refrigerator, the application of solar energy in adsorption refrigerators has widely been researched and studied by numerous researchers across the world. French scientists, Pons and Guilleminot (1986) studied activated carbon–methanol and zeolite–water adsorption systems driven by solar energy, where they obtained a COP of 0.12-0.14 an activated carbon–methanol ice maker with a collector area of 6 m^2 (four collectors) and adsorbent mass of 20–24 kg/m^2. A zeolite–water refrigerator studied by Grenier (1988) was about 0.10 with the collector area of 20 m^2 (24 collectors) and the adsorbent mass of 360 kg. K. Sumathy *et al*. (1999) studied a solar powered activated carbon–methanol ice maker in which he obtained a daily ice production of 4–5 kg and the COP was 0.1–0.2.

Apart from the usual solar collector-adsorption generator configuration, different types of collector-generator designs have been proposed. For example, Iloeje *et al*. (1997) utilized a tubular type of absorber, which used concentric metal pipes through which the adsorbent (such as calcium chloride, activated carbon) is filled. The inside of the concentric tube is used to pass the refrigerant fluid and the metal tube is attached to the collector surface.

Vasiliev (2005) proposed a design for a continuous adsorption heat pump with heat recovery provision than can be driven by both solar energy and natural gas. The system used a parabolic solar concentrator to capture solar energy which is used to heat a circulating stream of water. In doing so, it used solar energy as the main power supply, and natural gas served as an auxiliary heat source when solar energy was not adequate.

2.7.4 Development of novel adsorption working pairs

Adsorption working pairs are key element for adsorption refrigeration systems and decide the performance capability and efficiency. The thermal characteristics of the working complexes have significant influence on the COP of the system. In order for an adsorption refrigeration system to operate efficiently, the selection of adsorption refrigeration working pairs should be

based upon the heat source temperature and suitable refrigeration cycle times should also be selected based on the requirement of the refrigeration system.

Frequently used physical and chemical adsorption working pairs mainly include: metal hydrides-hydrogen, strontium chloride-ammonia and calcium chloride-ammonia, activated carbon-methanol, activated carbon fiber-methanol, activated carbon-ammonia, zeolite-water, silica gel-water, and so on (Srivastava and Eames, 1998). Composite adsorption, which is effective in heat and mass transfer intensification technology, is also proving to be a prospective technology for refrigeration.

In physical adsorption, the carbon-methanol working pair has a large adsorption and desorption concentration. Its desorption temperature is around 100°C which is suitable for applications of solar and low grade heat systems and also has the benefit of low adsorption heat, which is around 1800–2000 kJ/kg. It has also low sensitivity to temperature changes for adsorption capacity and it is generally used for higher heat source temperature.

For the working pair of silica gel–water, desorption temperature cannot be too high. If it is higher than 120°C, silica gel will be destroyed. Thus it is a common adsorbent for the low temperature heat source. On the contrary, zeolite-water working pair has a more wider range of desorption temperature (70–250 °C). Its adsorption heat is about 3200–4200 kJ/kg, and the evaporation latent heat of water is 2400– 2600 kJ/kg.

Zeolite–water is quite stable and won't be destroyed at a high temperature as opposed to that of silica gel. However, it has the disadvantages of a higher adsorption heat, which will lead to the low COP, as well as an evaporation temperature that needs to be higher than 0°C. In addition, the system is a vacuum system, which leads to a high requirement of vacuum sealing; meanwhile the low evaporation pressure also makes the adsorption process slower.

2.8 Selection criteria for various types of adsorption refrigeration systems

The selection of a specific type of adsorbent/refrigerant pair vastly depends on characteristics such as evaporator temperature, adsorption capacity of the adsorbent, adsorption heat, coefficient of performance and specific cooling power.

Table 2.1- Selection of adsorption refrigeration types

Type of refrigeration system	**Adsorbent/ Refrigerant**	**Evaporator temperature (°C)**	**Adsorption Capacity ($kg.kg^{-1}$)**	**Adsorption heat (kJ/kg)**	**COP**	**SCP (W/kg)**
Physical adsorption	AC,ACF/Methanol	8	0.29	1800-2000	0.3	140-500
	AC,ACF/R134a	5	1.29 - 2.2	1830-2300	0.38	214
	Silica Gel/Water	10	0.3	2500-2800	0.4	85
	Zeolite/Water	5	0.17	3200-4200	0.9	125
Chemical adsorption	$SrCl_2$-NH_3	-10	-	-	0.32	230
	Metal hydride/H_2	-10	-	-	0.43	25
Composite adsorbent	$CaCl_2$/activated carbon – ammonia	-15	-	-	0.41	731
	Activated carbon fiber/$CaCl_2$-NH_3	1	-	-	0.6	330

Hence, for selection purpose, table 2.1 presents the different types of adsorbent/refrigerant systems along with their properties. From the above table, we can see that there are three pairs of

refrigeration systems to choose from. Chemical adsorption systems have the shortcoming of agglomeration or particulate swelling where during adsorption and desorption processes there is a tendency for the system to form complex reactions that may not be reversible. Hence, chemical adsorption systems were not selected in this research work.

The second pair to be considered were, composite adsorbent systems. These refrigeration systems include the very best features of both physical and chemical adsorption refrigeration systems which makes the suitable for usage. As such, these systems are characterized by appreciable COP and SCP values that are suited for usage. However, these systems also incorporate the shortcomings of both physical and chemical adsorption refrigeration systems and were deemed not suitable for this research.

The third pair considered are physical adsorption refrigeration systems. In this system silica gel/water, zeolite/water and activated carbon/HCFC systems were taken into consideration. Zeolite/water systems are suitable for high temperature applications and their adsorption heat is very high with low adsorption capacity. Silica gel/Water systems operate with vacuum pressure and also have high adsorption heat requirement. Hence, by ruling out these two systems activated carbon/R134a was selected.

Chapter 3
Methodology

3.1 Description of methodology

In this chapter, the methodology for employing performance simulation of adsorption refrigeration is discussed in detail. The specific adsorption system used to analyze performance is activated carbon-R134a pair. This pair is selected based on a number of technical advantages over other kinds of adsorption pairs. Hence, from this point on, characterization of three types of activated carbons will be discussed. Afterwards, the performance of these pairs is discussed by comparing each performance indicators.

In order to carry out the simulation process, a specific method or flow of work has to be followed. This methodology flow work dictates how results can be achieved by following a framework from the start to the end of the research. The methodology is discussed in figure 3.1.

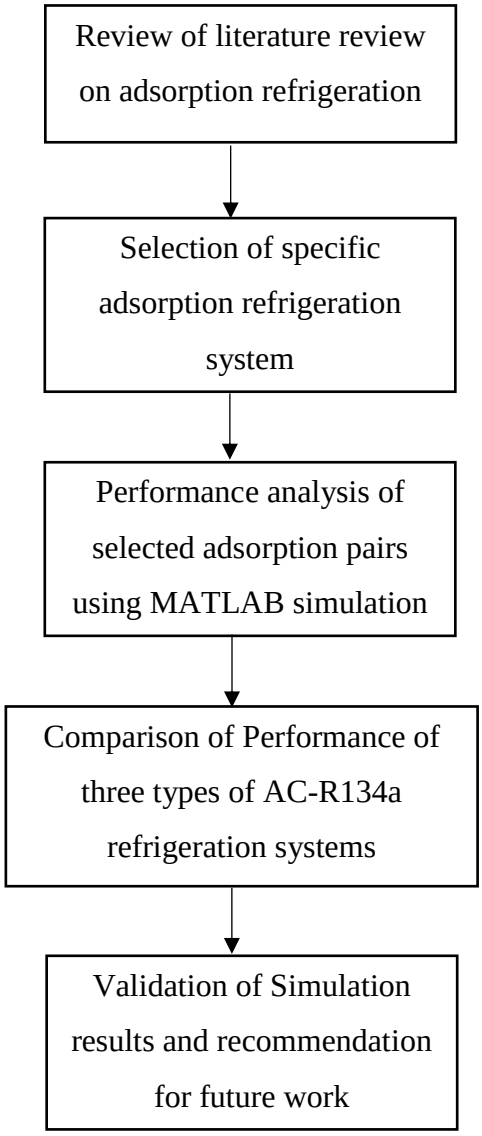

Figure 3.1 - Methodology of the research work

3.2 Description of the AC-R134a adsorption pairs

The analysis of the adsorption system takes into account three different types activated carbon-R134a types. These three varieties differ in the type of the activated carbon used namely; AC-A20, granular activated carbon and Maxsorb III. The constant values of n, E and W_o in the D-A equation are studied by different authors which are duly adopted in this paper. The material, surface properties and D-A equation constants of these varieties of activated carbon are listed in table 3.1.

Table 3.1 - Characteristics of Activated Carbon

AC type	A_{BET} ($m^2.g^{-1}$)	v_m ($cm^3.g^{-1}$)	d_p (n.m)	ρ ($kg.m^{-3}$)	E($J.mol^{-1}$)	Wo ($kg.kg^{-1}$)	n
Maxsorb III	3150	1.7	2	0.0022	7332.69	2.22	1.29
AC-A20	1930	1.05	2.16	0.0022	7136.01	1.29	1.49
Granular	900	0.88	2×10^6	510	9575	1.68	1.83

The design process begins first by determining the amount of R134 A required to convert the 2 kg/day of water to ice at -4^{o}C evaporator temperature which determines the cooling load. This helps to size the evaporator, condenser and adsorption-desorption bed.

3.3 Components of the adsorption bed

Before we begin the process of operation the first thing we have to do is construct the elements of the apparatus. For our specific case, a unique design has been used which incorporates additional structures and components. The purposes and uses of each of the components is described as follows.

Adsorber Bed

The adsorber bed is the main component that replaces the purpose of a mechanical compressor found in conventional vapor compression refrigerators. This adsorber bed contains a mixture of adsorbent and adsorbate adjusted to the right amount of ratio. In most designs, the bed of adsorbent adsorbate pairs is covered with double fiber glass covers since fiber glasses have better emissivity than glass and double covers reduce heat loss from the top section of the adsorbent bed.

The conditions of the adsorber bed are studied by measuring the temperature and pressure of the adsorber by installing pressure and temperature gauges on the top of the adsorber bed. An outlet is provided for the vapor to flow into the condenser and an inlet is also present for the vapor to come in from the evaporator and get adsorbed. This outlets or inlets are used one at a time during

operation to either let fluid into or out of the adsorber. A schematic representation of the adsorber design is given as follows.

In conjunction with the adsorber bed are fins that are used to improve heat transfer efficiency since the heat conductivity of activated carbon is very low. This is because it is an insulator that even though the adsorption capacity is appreciable.

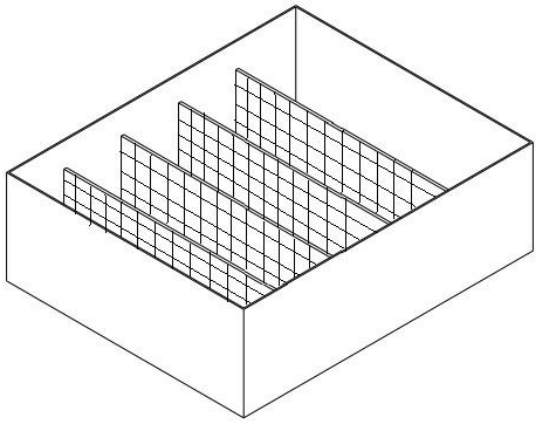

Figure 3.2 - Schematic view of the adsorber bed

The adsorber bed shown above in figure 3.2 is used to enhance the transfer of heat by easily capturing the heat coming out of the absorber plate and transferring it to the activated carbon/R134 pair which is placed right on top of the mesh fins. The meshing in the fins is preferred for the efficient diffusion of the refrigerant within the micro and mesopores of the activated carbon through which adsorption and desorption phenomenon is largely carried out. At the bottom of the adsorber bed is an opening for the refrigerant fluid to move out into the condenser.

Absorber plate

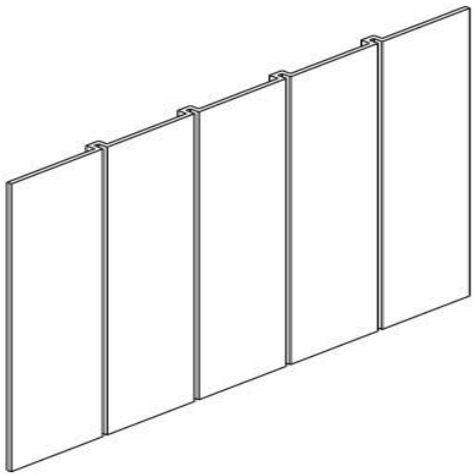

Figure 3.3 - Schematic view of Absorber plate

Shown in figure 3.3 is the schematic of the absorber plate which is used to absorb the solar radiation in the desorption phase of the system. This absorber is a black steel metal covered on top of the meshed fins in the adsorber bed. As shown in the figure, the plate has grooves at equal intervals of space which are fitted against the fins when the absorber is placed upon them.

3.4 Proposed Operation of the system

The proposed design of the solar adsorption refrigerator consists of a network of valves and components arranged in a way that makes the operation process smooth. Hence, figure 3.4 is given as an initial arrangement of system components of the refrigeration system.

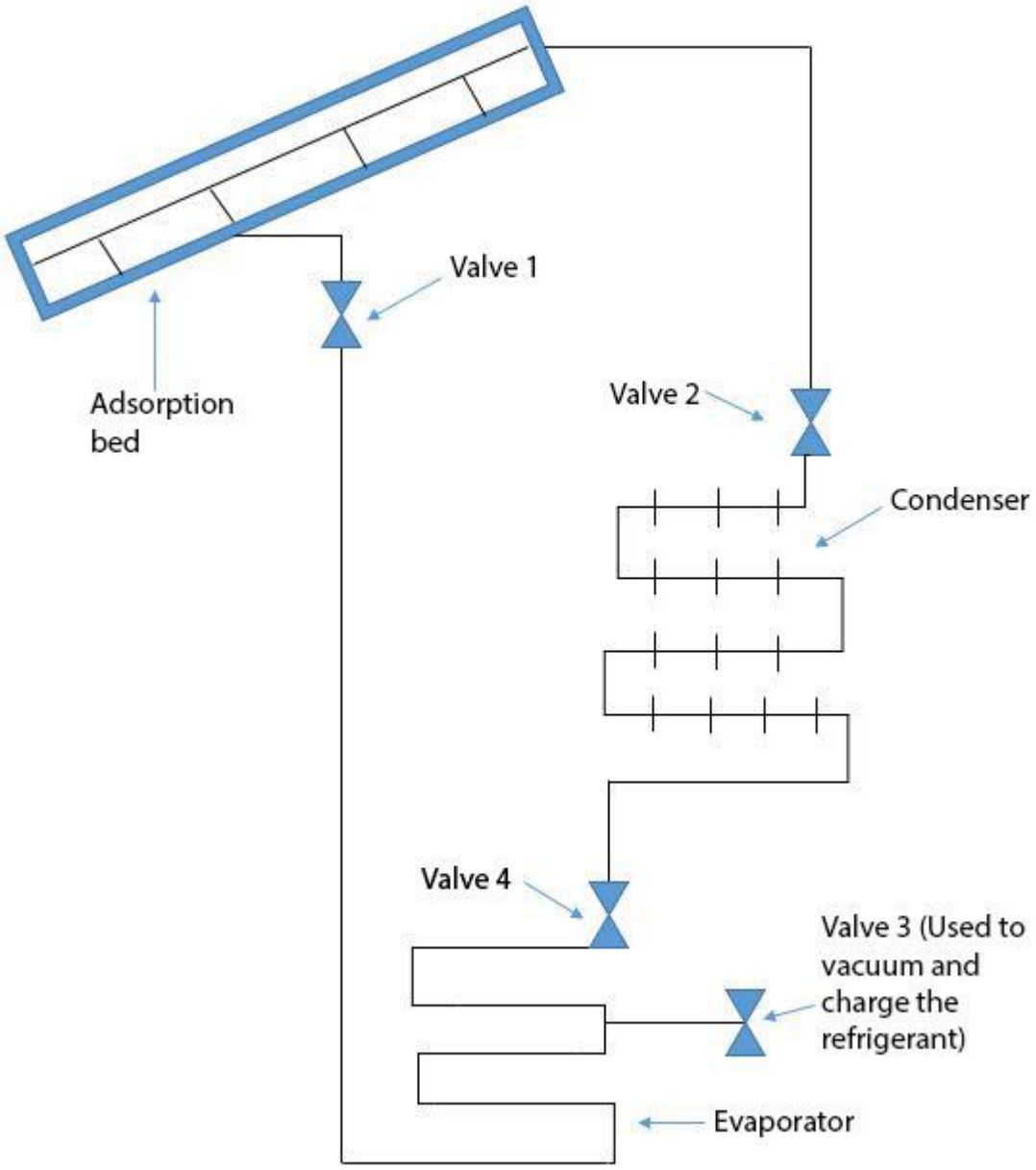

Figure 3.4 - Proposed design of the adsorption refrigeration system

The proposed design of the solar adsorption refrigerator consists of a network of valves and components arranged in a way that makes the operation process smooth. Hence, the above diagram is given as an initial arrangement of system components of the refrigeration system.

3.5 Simulation modelling of the Adsorption Refrigeration system

3.5.1 Adsorption simulation Modelling Equations

As discussed in the literature review, different empirical equations to relate pressure (p), temperature (T) and concentration (W) are suggested by various researchers. Since Dubinin-Asthakov equation considers microporous adsorption phenomena it to be used to describe adsorption characteristics in this paper. The adsorption equations for the three types of adsorbents is represented as follows. The general Dubinin-Asthakov equation is represented as follows.

$$W = W_o \, exp\left(-\left(\frac{RT}{E} ln\left(\frac{P_s}{P}\right)\right)^n\right) \qquad \text{(eq. 3.1)}$$

Where

W Concentration at a given temperature (T) and pressure (p), kg adsorbate/kg of adsorbent

W_o Maximum adsorption capacity (concentration), kg adsorbate/kg of adsorbent

E Characteristic energy, J/mol

T Absolute temperature of adsorption bed, K

P Pressure of adsorption bed, Pa

P_s Saturation pressure of refrigerant at temperature, T

R Universal gas constant, kJ/mol.K

n exponential constant

While the D-A equation is mainly used in the simulation program, other equations are also used to support the simulation process. One of these equations is the Antoine equation which is used to estimate the saturation pressure of the refrigerant R134a at any given temperature and it is given as follows.

$$lnP_s = A - \frac{B}{T-C} \qquad \text{(eq. 3.2)}$$

Where, P_s = saturation pressure, kPa

A = Constant of Antoine equation, 14.41

B = Constant of Antoine equation, 2094

C = Constant of Antoine equation, 33.06

The adsorption refrigeration process consists of isosteric heating, isobaric desorption, isosteric cooling, and isobaric adsorption. The consecutive occurrence of these processes forms one complete adsorption cycle. The cycle starts at a point where the refrigerant is absorbed in the adsorbent. From here, the total energy gained by the system during the heating period is the sum of energy from point 1 to 2, Q_{12} (isosteric heating) and energy from 2 to 3, Q_{23} (isobaric desorption). These two energies can be calculated as follows.

$$Q_{12} = (m_a C_{p,a} + C_{p.R134a} m_{R134a} (T_2 - T_1) + m_f C_{p,s}(T_2 - T_1) + m_{a,p} C_{p,s}(T_2 - T_1) + m_{bed} C_{P,s}(T_2 - T_1) \quad \text{(eq. 3.3)}$$

$$Q_{23} = \left(m_a C_{p,a} + C_{p,R134a} m_a \left(W_1 + W_3/2\right)\right) \times (T_3 - T_2) + (W_1 - W_3)H + m_f C_{p,s}(T_3 - T_2) + m_{a,p} C_{p,s}(T_3 - T_2) + m_{bed} C_{P,s}(T_3 - T_2) \quad \text{(eq. 3.4)}$$

$$H = RC.\frac{T}{T_2} \quad \text{(eq. 3.5)}$$

$$Q_e = (W_1 - W_3) \times h_{fg} \quad \text{(eq. 3.6)}$$

$$COP = \frac{Q_e}{Q_{12}+Q_{23}} \quad \text{(eq. 3.7)}$$

$$COP_{solar} = \frac{Q_e}{Q_{rad}} \quad \text{(eq. 3.8)}$$

$$SCP = \frac{((W_1 - W_3) \times h_{f,g} + (m_{R134a} \times C_{p,R134a}(T_3 - T_1)))}{t_{cycle}} \quad \text{(eq. 3.9)}$$

Where,

Q_{12} = Isosteric heating energy, kJ

Q_{23} = Isobaric desorption heating energy, kJ

Q_e = Cooling effect, kJ

Q_{rad} = total heat collected from solar radiation, J

$C_{p,a}$ = specific heat capacity of activated carbon, kJ/kg.K

$C_{p,R134a}$ = specific heat capacity of R134a, kJ/kg.K

$C_{p,s}$ = specific heat capacity of steel, kJ/kg.K

m_a = mass of activated carbon, kg

m_f = mass of fins, kg

$m_{a,p}$ = mass of absorber plate, kg

m_{bed} = mass of adsorber bed, kg

W_1 = adsorption capacity (concentration) of bed at the start of isosteric heating, $kg.kg^{-1}$

W_3 = adsorption capacity (concentration) of bed at the end of isobaric desorption, $kg.kg^{-1}$

T_1 = Temperature of bed at the start of isosteric heating, K

T_2 = Temperature of bed at the end of isosteric heating, K

T_3 = Temperature of bed at the end of isobaric desorption, K

H = Isosteric heat of desorption, kJ/kg

h_{fg} = latent heat of vaporization of R134a, kJ/kg.K

COP = coefficient of performance

COP_{solar} = solar coefficient of performance

SCP = specific cooling power, W/kg

t_{cycle} = cycle time required to deliver Q_e

3.6 Description of AC-R134a pair types

3.6.1 D-A equation for ACF-A20-R134a pair

The D-A equation describes how the adsorbate concentration at any instant within the adsorption bed varies. In order to understand the interaction of adsorbate and adsorbent, values of the characteristic energy E, exponential constant and the maximum adsorption capacity,W_o should be determined. For ACF-A20-r134a adsorption pairs these values were determined to be 7136.01 J.mol^{-1}, 1.49 and 1.29kg.kg^{-1}(**Loh et. Al, 2012**). Hence, from these values the D-A equation that characterizes adsorbate-adsobent interaction for this specific pair is given as in the following equation.

$$W = 1.29 \times \exp\left(-\left(0.001165 \times T \times ln\left(\frac{P_s}{P}\right)\right)^{1.49}\right) \quad \text{(eq 3.10)}$$

Hence, using the above equation it is possible to draw the adsorption isotherm and the p-T-W diagram. The adsorption isotherm and p-T-W diagrams will be given in the results section of this paper.

3.6.2 D-A equation for Granular AC-R134a pairs

In a same way as to that of ACF-A20-R134a pairs, the D-A equation constant values have been well-studied and determined accordingly. The values of corresponding to the D-A equations are; characteristic energy, E, 9575 J.mol^{-1}, exponential constant, n, 1.83 and the maximum adsorption capacity (concentration), W_o, 1.68 kg.kg^{-1}. Substitution of these values gives the complete D-A equation for this specific adsorbate-adsorbent pairs which is given as follows.

$$W = 1.68 \times \exp\left(-\left(0.000868 \times T \times ln\left(\frac{P_s}{P}\right)\right)^{1.83}\right) \quad \text{(eq. 3.11)}$$

With the aid of the above equation and the clausius-clapeyron equation, it is possible to draw both the adsorption isotherm and p-T-W plots.

3.6.3 D-A equation for Maxsorb III-R134a pairs

The third type of activated carbon adsorbent is the Maxsorb III which has the highest adsorption capacity as compared to ACF – A20 and granular AC adsorbents. The constants of Maxsorb III-R134a for the corresponding D-A equation are; characteristic energy, E, 7332.69 $J.mol^{-1}$, exponential constant, n, 1.29 and the maximum adsorption capacity (concentration), W_o, 2.22 $kg.kg^{-1}$ (**Loh et al., 2012**). Substitution of these values gives the complete D-A equation for this specific adsorbate-adsorbent pairs which is given as follows.

$$W = 2.22 \times \exp\left(-\left(0.001134 \times T \times ln\left(\frac{P_s}{P}\right)\right)^{1.29}\right) \quad \text{(eq. 3.12)}$$

With the aid of the above equation and the clausius-clapeyron equation, it is possible to draw both the adsorption isotherm and p-T-W plots.

Chapter 4
Results and Discussion

In this chapter, the results of the simulation test for each type of activated carbon-R134a pair are presented and analyzed. The results will clearly show how each type of adsorbate-adsorbent pair behave and perform under different operating conditions. Hence, the findings presented in this chapter can be used as guidelines to selecting the best performing adsorbate-adsorbent pair for cooling systems. These results may also serve as baseline information for further research and development endeavors on the adsorption behavior and performance of other types of activated carbon and R134a pairs.

The study mainly focuses on the performance analysis. First, the cycle diagrams of each pair are studied for fixed operating conditions. This will give a clear picture of how each process of isosteric heating/cooling, isobaric desorption/adsorption takes place. This simulation result can then be used as a guideline to compare it with experimental testing of the refrigeration/chilling process.

Secondly, results of COP against varying generation temperature values are analyzed. This is important since such analysis can help decide which operating conditions are optimum for a specific refrigeration/chilling application. Hence, using five different adsorption outlet temperatures of the adsorption bed (i.e. temperature value at T_1), change of COP with varying amounts of generation temperature/T_3 is studied for every type of adsorption pairs. The results of the analysis will be discussed in detail in this chapter.

The variation of COP with W_3 ($W_{minimum}$) were also studied. As with the case of COP vs generation temperature, the COP values were drawn against values of W_3 using the five different values of bed outlet temperature. The values of SCP were also equally important in analyzing the performance of the adsorption refrigeration system. Hence, the results of SCP were again compared with the corresponding values of generation temperature.

The SCP values were again drawn versus the values of W_3 ($W_{minimum}$). This helps to holistically understand the relationship of SCP against changing the temperature of generation and the values of $W_{minimum}$. In this way, it is possible to understand and choose optimum operating

conditions for the system under study. Lastly, the values of solar COP were calculated. For every respective month the average value of the solar radiation was taken and used to calculate the obtainable solar COP values. Hence, a proper comparison between the values of cycle COP and solar COP will be made from the values obtained. The paper culminates by comparing each performance parameters for the three types of adsorbate-adsorbent pairs and suggesting the best and most effective pair and recommendations on how to further develop the study.

4.1 Adsorption Isotherms and p-T-W diagrams

The properties of adsorbate/adsorbent pairs can be easily indicated using either isotherm chart or pressure-Temperature-Concentration (P-T-W) chart. The characteristics results of the three pairs are discussed below.

4.1.1 Adsorption isotherm and p-T-W diagrams for ACA-F20

From isotherm figures it is possible to understand that as the temperature within the adsorbent is increased the amount of adsorbate concentration within the bed decreases. Hence, it can be deduced that lower adsorbent temperature is preferred in order to accomplish effective adsorption and higher temperature values are preferred for desorption operations. Also, the adsorption diagram can also show the maximum pressure that could be fixed to the solar adsorption bed up to the point of saturation. After the pressure, P equals that of saturation pressure, liquid starts to form in the bed and the D-A equation will no longer be applicable. This will be limited by the type of cooling medium used to condense the desorbed refrigerant. Further heating will not increase pressure but keep the generated vapor to be condensed and collected in the condenser which is located outside the bed.

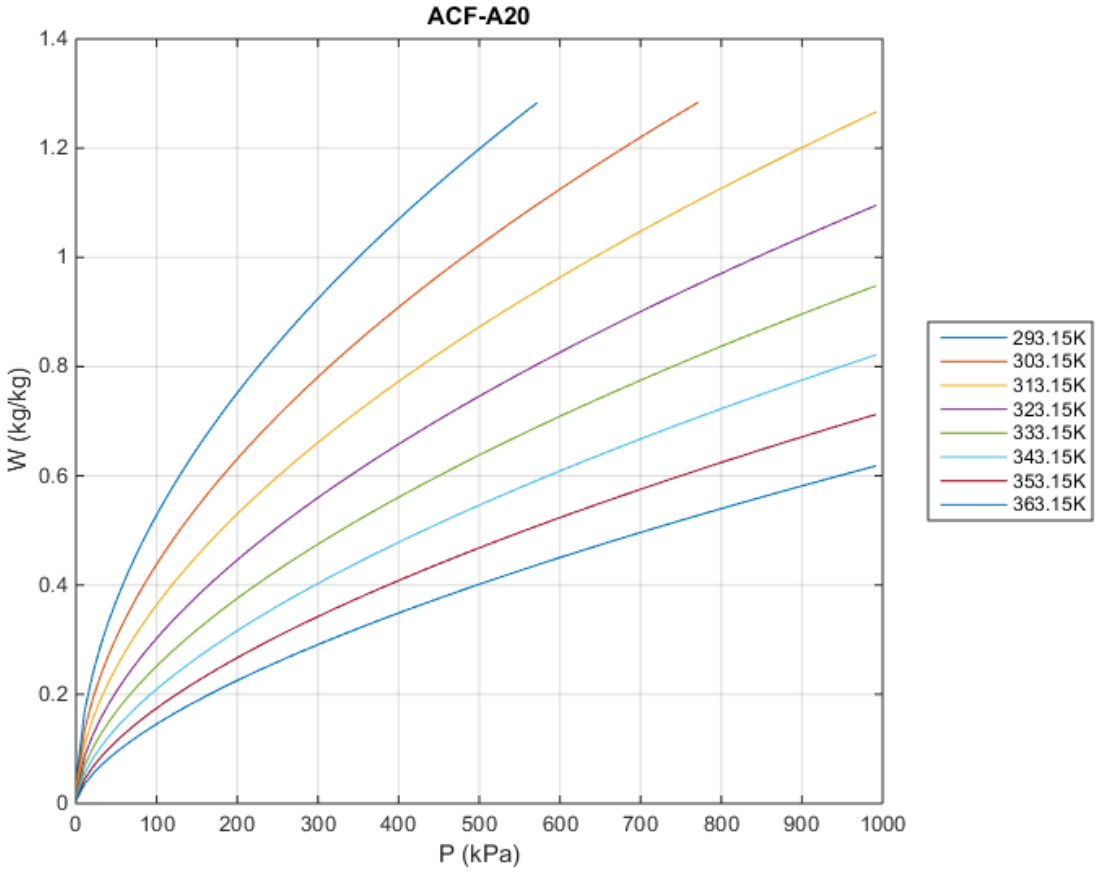

Figure 4.1 - Adsorption isotherm for ACA-F20-R134a pairs

Figure 4.1 shows the relationship among pressure, temperature and concentration of adsorbate in the adsorbent. The isotherm is drawn for temperature ranges of 293-363K. As shown in the chart the highest adsorption capacity is observed at 20°C (293K). At this point a maximum adsorption concentration of 1.28 $kg.kg^{-1}$. As the temperature increased maximum adsorption capacity decreased from 1.28 to 0.618 $kg.kg^{-1}$ at 90°C (363K). The pressure at 363K was 991kPa.

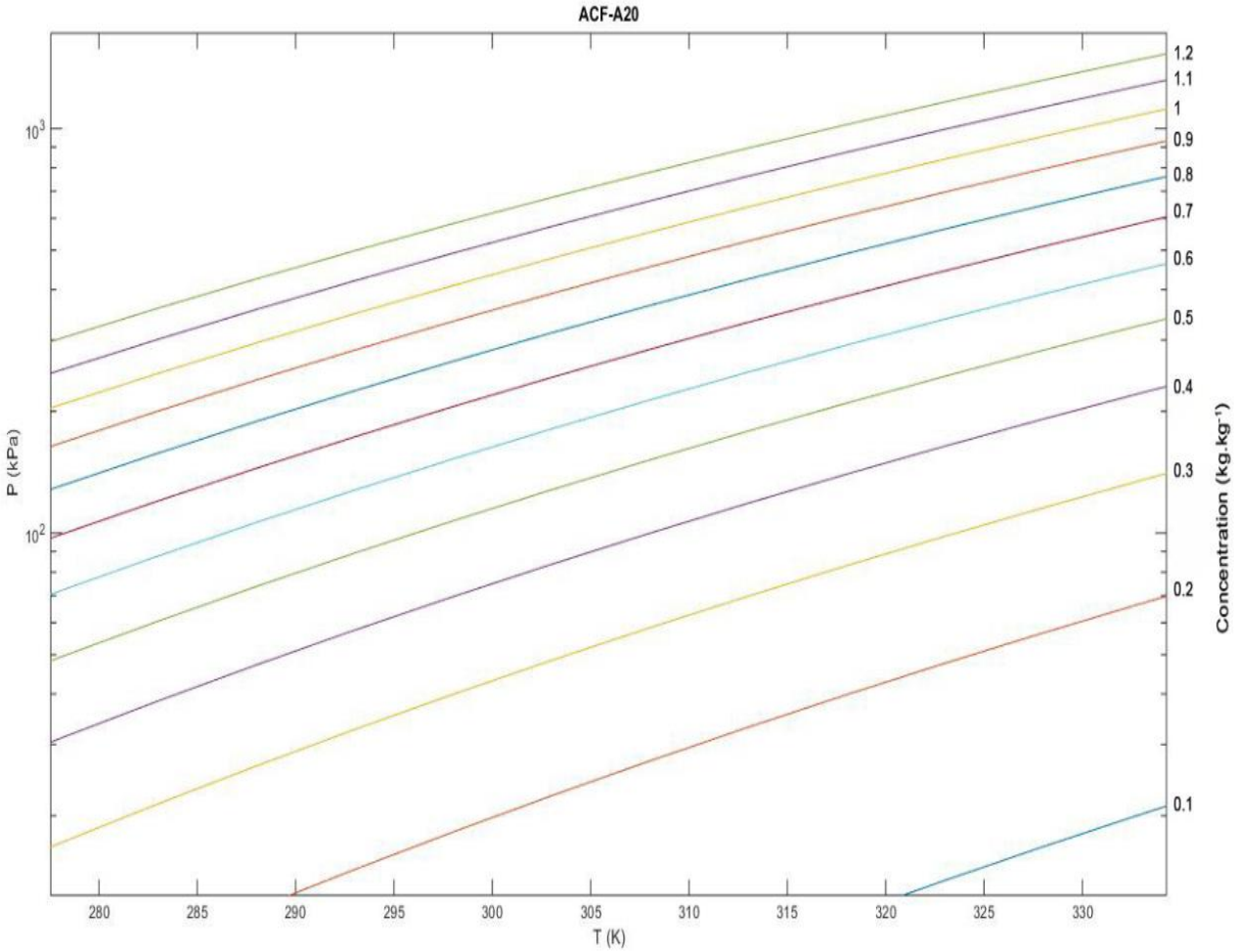

Figure 4.2 - p-T-W diagram of ACF-A20-R134a pairs

Another important relationship exists among the pressure, P, temperature T and adsorbate concentration W. Figure 4.2 illustrates how concentration of the adsorbate is affected by pressure and temperature. For example, by raising the pressure from 300 upto 1000 kPa and beyond while also manipulating the temperature, adsorbate concentration of 1.2kg.kg^{-1} can be sustained. Hence, for any given temperature and pressure value, constant adsorbate concentrations can be read from the above figure. This is helpful to maintain required refrigerant in adsorption bed. Hence, the chart can help to determine the two states of the heating (desorption) process and the concentration change can easily be calculated. Concentration change is proportional to the cooling (refrigeration) effect.

4.1.2 Adsorption isotherm and p-T-W diagrams for Granular AC

The adsorption isotherm chart of granular AC-R134a pairs is given as in the following figure by varying the pressure for a certain temperature value and finding adsorbate concentration. Figure 4.3 shows the temperature curve diverges from the origin.

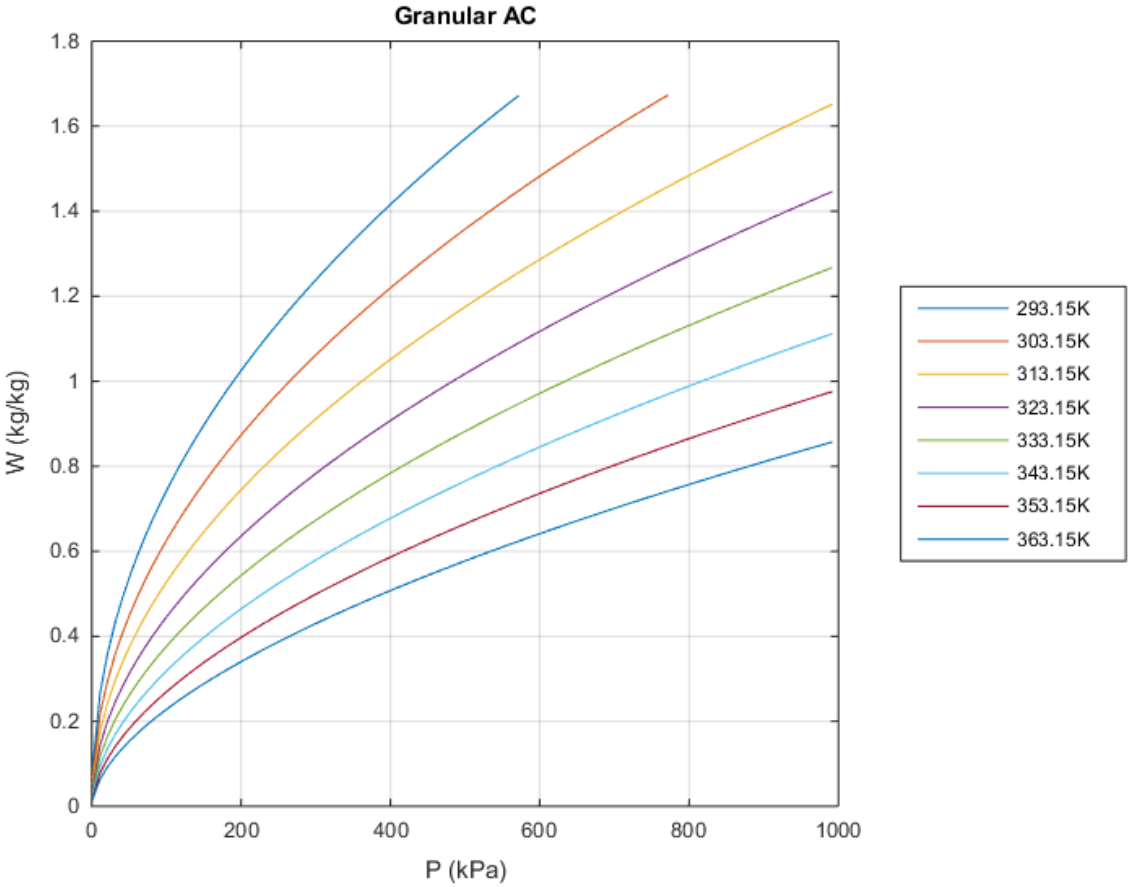

Figure 4.3 - Adsorption Isotherm diagram for Granular AC-R134a pairs

As seen in figure 4.3, as the temperature of the adsorption increases from 20-90°C, the amount of refrigerant adsorbed on to the surface of granular activated carbon decreases from the highest value at 1.68 to 0.857kg.kg^{-1}. This is essential in selecting an appropriate temperature and pressure ranges for favorable operating conditions of the refrigeration system. Depending on the specific operating conditions, by trading off the temperature and pressure values it is possible to decide the amount of refrigerant required for a specific refrigeration operation.

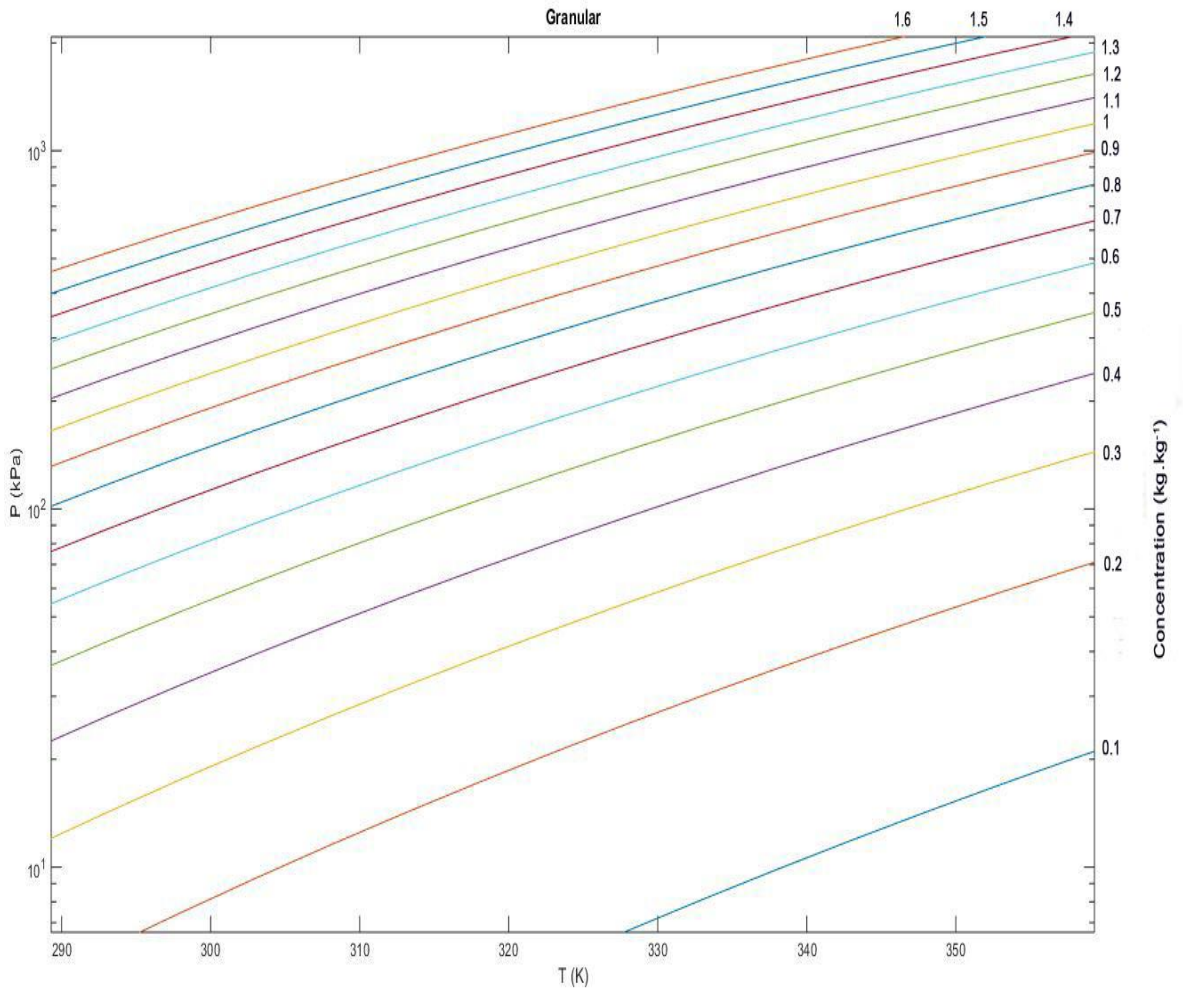

Figure 4.4 - p-T-W diagram of granular AC-R134a pairs

As seen from figure 4.4, maximum adsorption capacities are obtained when the pressure in the adsorbent-adsorbate pairs is above the range of 400kPa. Hence, the economical nature of operating in these pressure ranges should be duly studied. Generally, for chilling purposes, operating between 10 up to 200 kPa is suitable since high adsorbate amount is not necessarily required since the cooling effect is low. However, when refrigeration is needed required adsorbate amount and pressure increase, hence the need to operate in high pressure ranges.

4.1.3 Adsorption isotherm and p-T-W diagrams for Maxsorb III

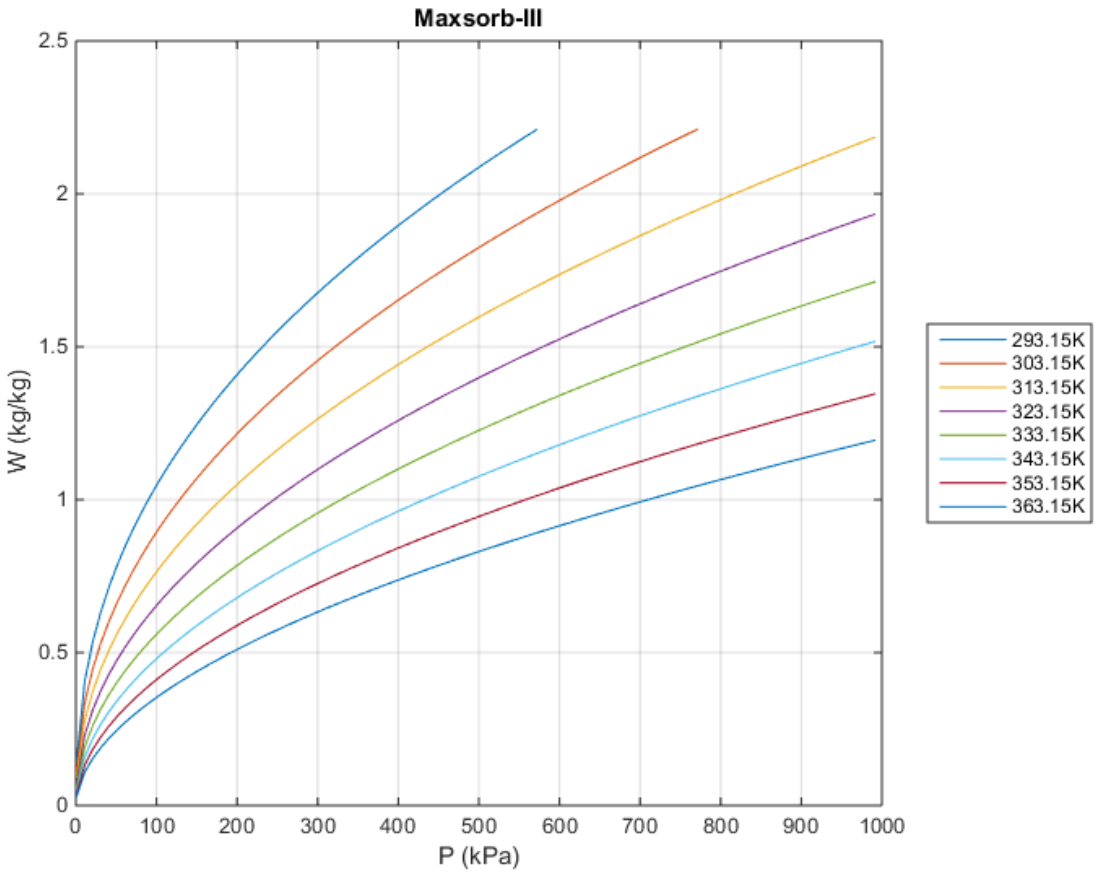

Figure 4.5 - Adsorption isotherm for Maxsorb III-R134a pairs

The above graph illustrates how the adsorption for Maxsorb III adsorbent proceeds under different operating conditions. From figure 4.5, it is apparent that the maximum adsorption condition occurs at 293.15K and a pressure value of 571kPa. The lowest adsorption capacity observed for the highest pressure value was 1.194kg.kg^{-1} at a pressure value of 991kPa and temperature of 90°C (363K). This is due to the fact that at high temperature values the adsorption capacity decreases since the adsorption bed is more inclined to desorption than adsorption. Also, at higher temperature values, pressure can be increased up to higher values since the saturation pressure is also very high. Hence, as per desired operation condition one can choose at which temperature, pressure and concentration values the refrigeration/chilling process takes place.

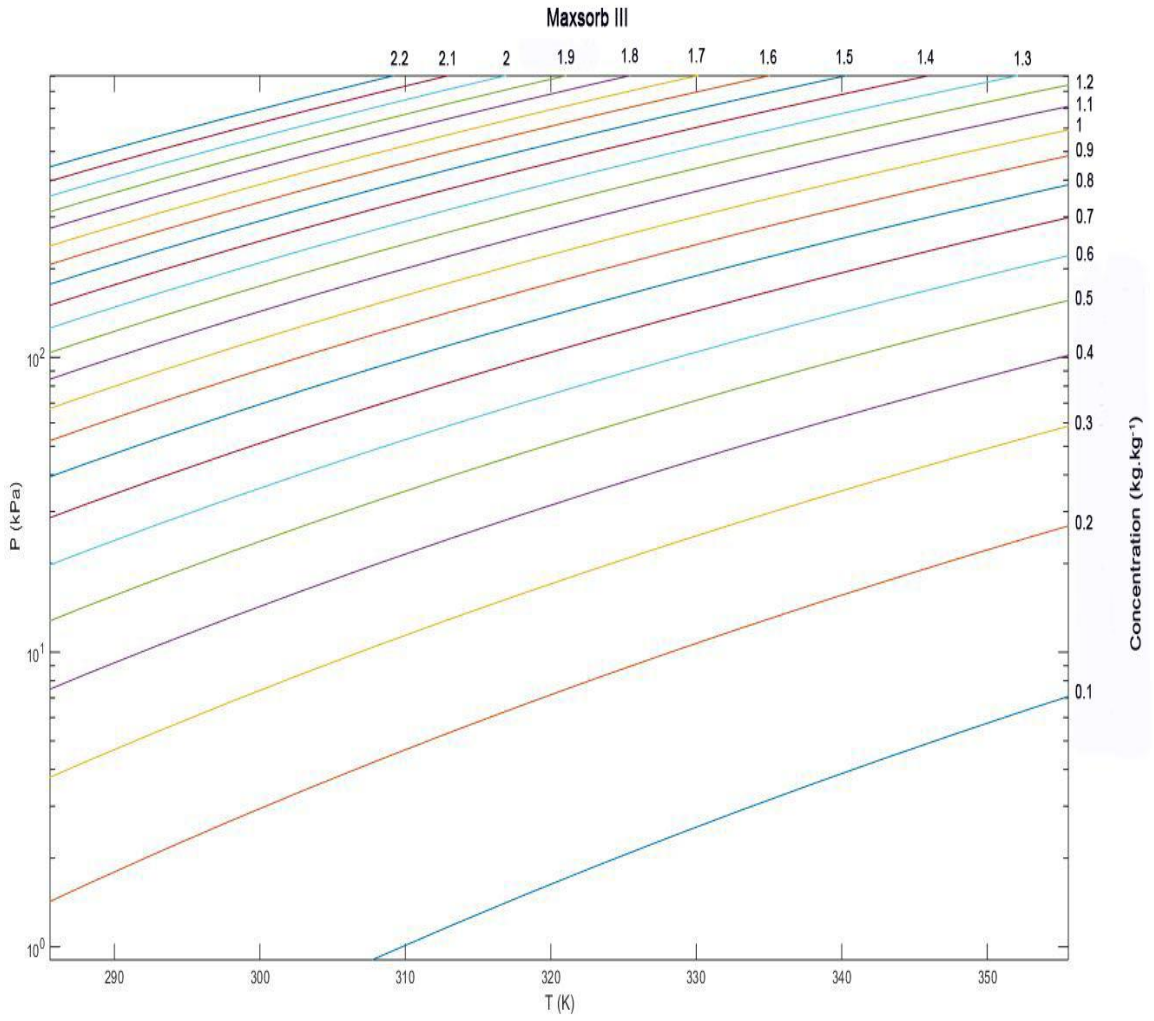

Figure 4.6 - p-T-W diagram for Maxsorb III-R134a pairs

The p-T-W diagram for Maxsorb III-R134a pair is as shown in figure 4.6. This specific adsorbent has the maximum adsorption capacity of 2.2kg.kg^{-1} in the pressure ranges of 400kPa and above. This will be suitable for applications of refrigeration/chilling where high amount of cooling effect is required. It is also suitable for low cooling effect operations since at lower pressure and temperature ranges the amount of concentration decreases. Hence, this adsorbent type is suitable for both chilling and refrigeration applications in its nature.

4.2 cycle diagrams of activated carbon-R134a pairs

The refrigeration cycle diagrams of the three variants of adsorption pairs are given in this section. Specific operating conditions were selected for each type of physical adsorption systems and the characteristics of the adsorption systems under adsorption and desorption conditions was studied. The operating conditions selected were P_c = 600kPa and P_e=270kPa. The reason behind it is that the operating pressures of AC/R134a pairs are positive pressure and at these selected values a higher adsorbate concentration can be adsorbed inside the adsorption bed. This allows for the chilling operation to proceed smoothly. At 600kPa $T_{a,i}$ = 318K and at P_e=270kPa $T_{a,o}$=308K due to the D-A equation used. $T_{g,o}$ = 348K since the application of the refrigeration system is only for chilling purpose. Higher values of $T_{g,o}$ are used for refrigeration purposes.

4.2.1 Cycle diagram for ACF-A20

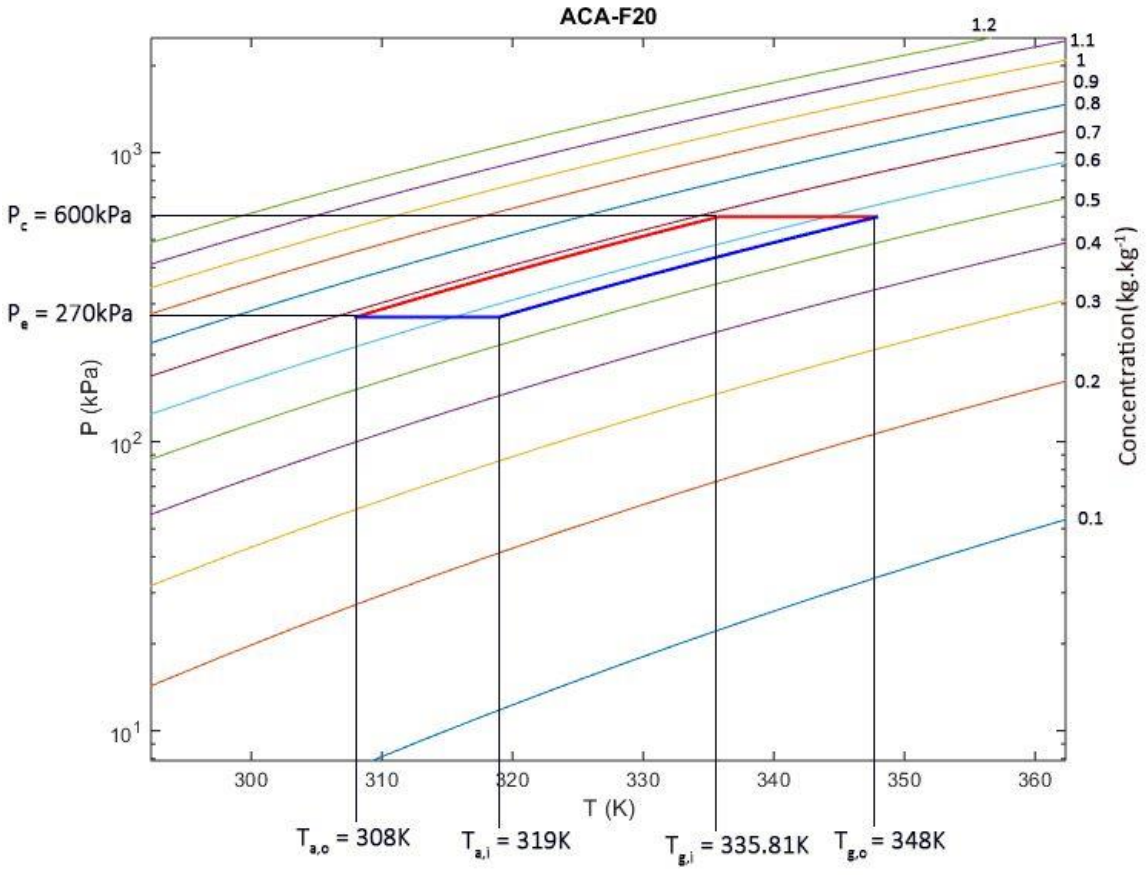

Figure 4.7 - Cycle diagram for ACF-A20

Figure 4.7 clearly shows what takes place in the adsorption refrigeration bed for activated carbon ACA-F20-R134a pair when the adsorption complex is heated from an initial bed outlet temperature, $T_{a,o}$ of 308K up to regeneration temperature, $T_{g,o}$ of 348K. Operating temperature and pressure ranges were selected to depict how the system performs under the selected conditions. Therefore, the operating conditions, P_e = 270kPa and P_c = 600kPa were selected arbitrarily to be evaporator and condenser pressure values of the refrigeration/chiller system.

In the graph, at a $T_{a,o}$ value of 308K the isosteric heating (desorption) process starts. At this point the concentration of the refrigerant at this point is calculated and was found to be 0.6808 $kg.kg^{-1}$. This value is indicated with dotted blue lines on the upper side of the cycle diagram. The bed is heated to the final isosteric temperature, $T_{g,i}$ of 335.81K. At this temperature, the condenser pressure of 600kPa is reached and the isosteric heating ends and replaced by isobaric desorption process until the temperature reaches 348K.

During this step, the refrigerant concentration in the bed decreases slowly up to the point of regeneration temperature. At this point the final concentration of the refrigerant R134a was found to be 0.5659 $kg.kg^{-1}$. Hence, the refrigeration effect created is equal to the difference between the concentrations at isosteric heating and isobaric desorption. This value was found to be 0.1149 $kg.kg^{-1}$. Further heating can decrease the concentration up to 0.5$kg.kg^{-1}$ but the operating conditions limit further process of isobaric desorption.

After the cycle is heated up to the regeneration temperature, the next phase of operation will be decreasing the temperature of the bed or isosteric cooling. During this process, the temperature of the bed is decreased isosterically at a constant concentration of 0.5659 $kg.kg^{-1}$ until its pressure attains that of evaporator pressure at 270kPa. In the simulation process, this decrement of temperature proceeded up to the temperature of $T_{a,i}$ at 319K. During the isosteric cooling process the temperature of the bed decreases and adsorption of R134a on to the bed begins. This process also slightly increases the concentration of the refrigerant inside the bed.

The final process of the adsorption begins when the amount of refrigerant begins increasing until it reaches its initial concentration of 0.6808 $kg.kg^{-1}$. At this point the temperature of the

bed decreases from 319K up to 308K thereby creating a conducive environment to carry out adsorption. The decreasing level of pressure also helps the adsorption process in the previous isosteric cooling and thus combined effect of decreasing pressure and temperature help the bed regain its initial concentration. The complete process of isosteric heating/cooling and isobaric heating/cooling creates one cycle of refrigeration. Hence, in order to attain a desired level of cooling the cycle time can again be repeated multiple times.

4.2.2 Cycle diagram for Granular AC-R134a

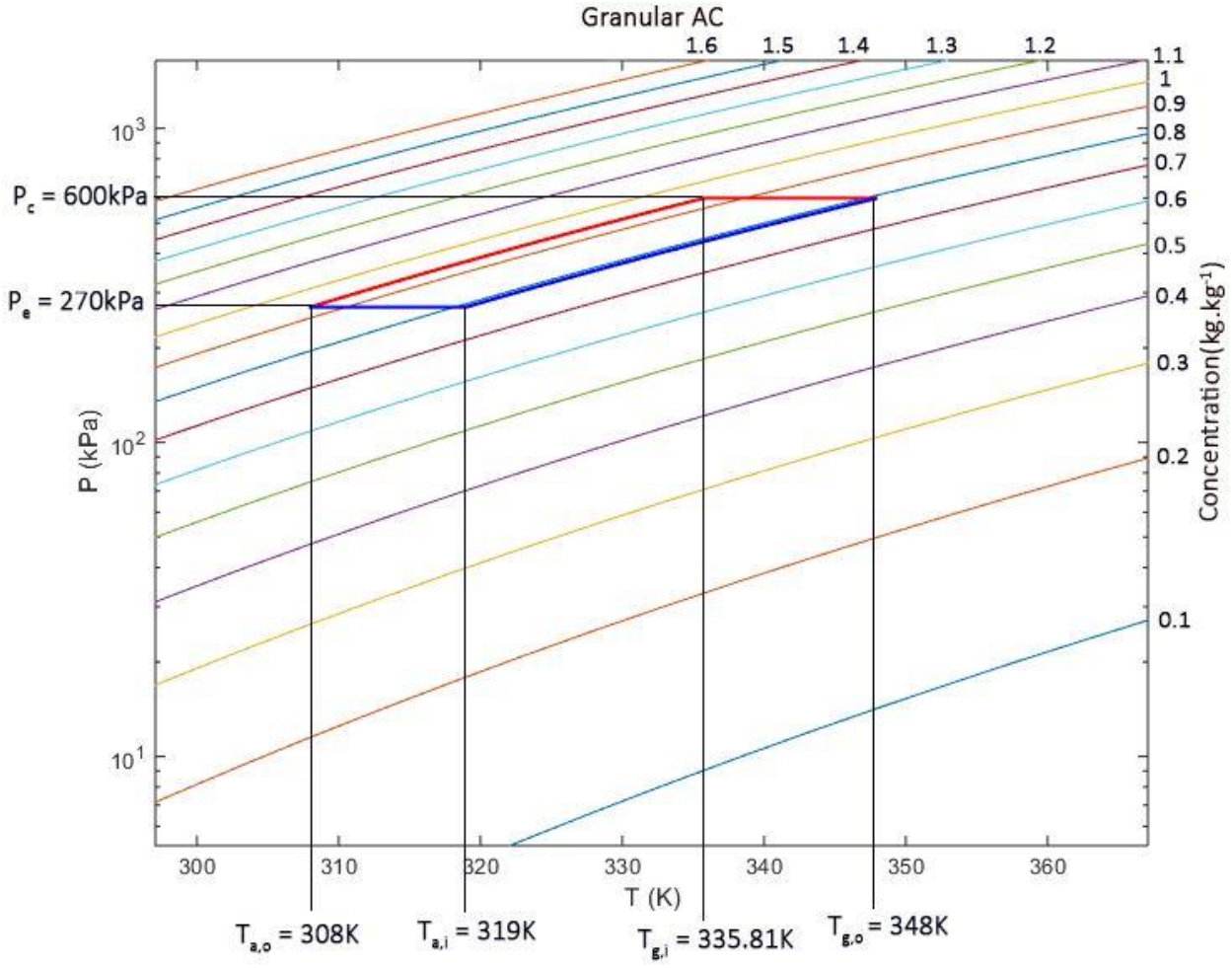

Figure 4.8 - Cycle diagram for Granular AC-R134a

In a similar fashion as to that of ACA-F20-R134a, figure 4.8 shows how the adsorption refrigeration process of granular activated carbon takes place when the adsorption pair is heated from an initial bed outlet temperature, $T_{a,o}$ of 308K up to regeneration temperature,$T_{g,o}$ of 348K.

The same process conditions were selected as the ACA-F20 adsorbent so that it can be easier to analyze both systems based on the same standpoint. Therefore, the operating conditions, P_e = 270kPa and P_c = 600kPa were selected arbitrarily to be evaporator and condenser pressure values of the refrigeration/chiller system.

In the cycle diagram of granular activated carbon adsorbent, at a $T_{a,o}$ value of 308K the isosteric desorption process starts. At this point the concentration of the refrigerant is calculated and was found to be 0.9361 $kg.kg^{-1}$. This value is indicated with dotted blue lines on the upper side of the cycle diagram and it shows an increment to that of ACA-F20 adsorbent by a margin of 0.2823 $kg.kg^{-1}$. Hence, this value shows that under the same operating conditions the granular activated carbon has more capacity of adsorption than ACA-F20 adsorbent. From this starting point the isosteric heating begins and the bed is eventually heated to the final isosteric temperature, $T_{g,i}$ of 335.81K and condenser pressure of 600kPa.

At the beginning of the isobaric desorption, the bed starts losing concentration. Desorption is carried out from a temperature value of 335.81K until the regeneration temperature $T_{g,o}$ value of 348K is reached by the bed. At this point the final concentration of the refrigerant R134a was found to be 0.7904 $kg.kg^{-1}$. Hence, the refrigeration effect created is equal to the difference between the concentrations at isosteric heating and isobaric desorption. This value was found to be 0.1457 $kg.kg^{-1}$. The amount of refrigerant desorbed at the end of regeneration process has a 0.03 $kg.kg^{-1}$ increment when compared to ACA-F20 adsorbent. Further heating can decrease the concentration up to 0.7$kg.kg^{-1}$ but achieving this value requires more heat input since this value can be reached at temperature ranges of around 360K. It will consequently increase the cycle time which may not be preferred in some applications.

During isosteric cooling the temperature of the bed is decreased from 348K up to 319K. This process is carried out at a concentration of 0.7904 $kg.kg^{-1}$. The pressure of the bed is allowed to decrease up to evaporator pressure of 270kPa from which the adsorption of R134a into the

adsorption bed begins. Further cooling of the bed to the initial value of $T_{a,o}$ 308K helps it regain the initial concentration of 0.9361 $kg.kg^{-1}$. As in the previous case, this process can be repeated multiple times so that the desired level of refrigeration/chilling effect can be created on the material being cooled.

4.2.3 Cycle diagram for Maxsorb III-R134a

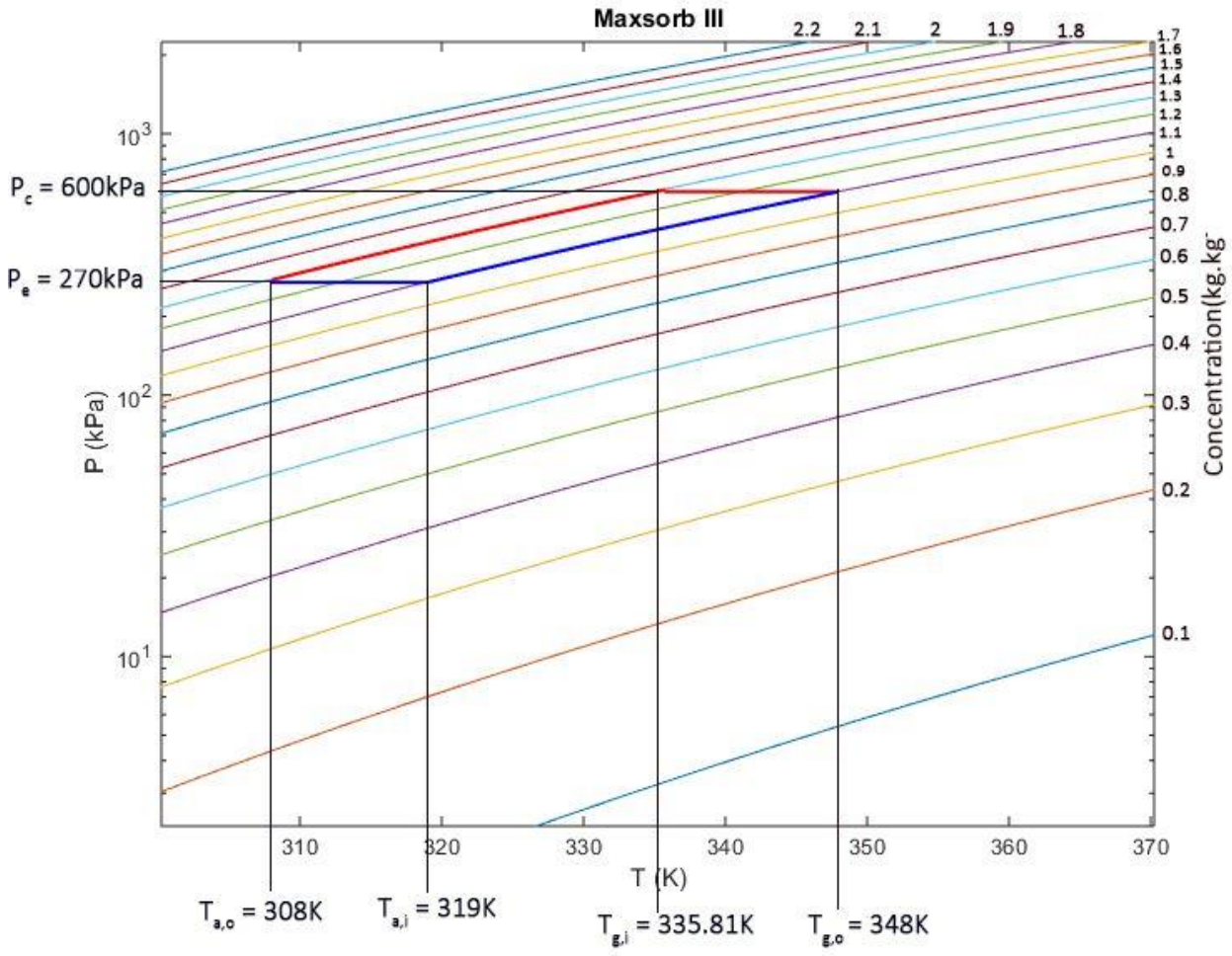

Figure 4.9 - Cycle diagram for Maxsorb III-R134a

Figure 4.9 is a cycle diagram for Maxsorb III-R134a pairs. The same operating conditions are selected as the rest of the adsorbate-adsorbent pairs. The main difference from the above two is the adsorption capacity observed at the end of desorption. Since this type of adsorbent has

the maximum adsorption capacity as compared to the other two types, the desorbed amount of R134a at the end of the isobaric desorption is expected to be higher.

In the isosteric heating/pressurization process, the bed is heated from 308K to 335.81K under a constant concentration of 1.2955kg.kg^{-1}. From this point on isobaric desorption takes over up to 348K. At the end of this desorption process the final concentration of the refrigerant is 1.1085 kg.kg^{-1}. At the end of the desorption process the desorbed amount of refrigerant is 0.187 kg.kg^{-1}. This value has a 0.0413 kg.kg^{-1} increment as compared to granular AC-R134a pairs and a 0.0721 kg.kg^{-1} increment when compared to ACF-A20-R134a pair. From the diagram it can be observed that further increase in the desorption temperature can lead to final desorption concentration of 0.9 kg.kg^{-1}.

Hence, from the results of simulation it is evident that Maxsorb III has the largest adsorption capacity under the same operating conditions which is due to its high surface area, pore volume and small particle diameter which all work in favor of its high adsorption capacity and hence effectiveness in refrigeration/chilling operations.

4.3 Comparison of Performance indicators

4.3.1 Cycle COP vs Generation temperature

4.3.1.1 Cycle COP vs Generation temperature for ACF-A20-R134a pair

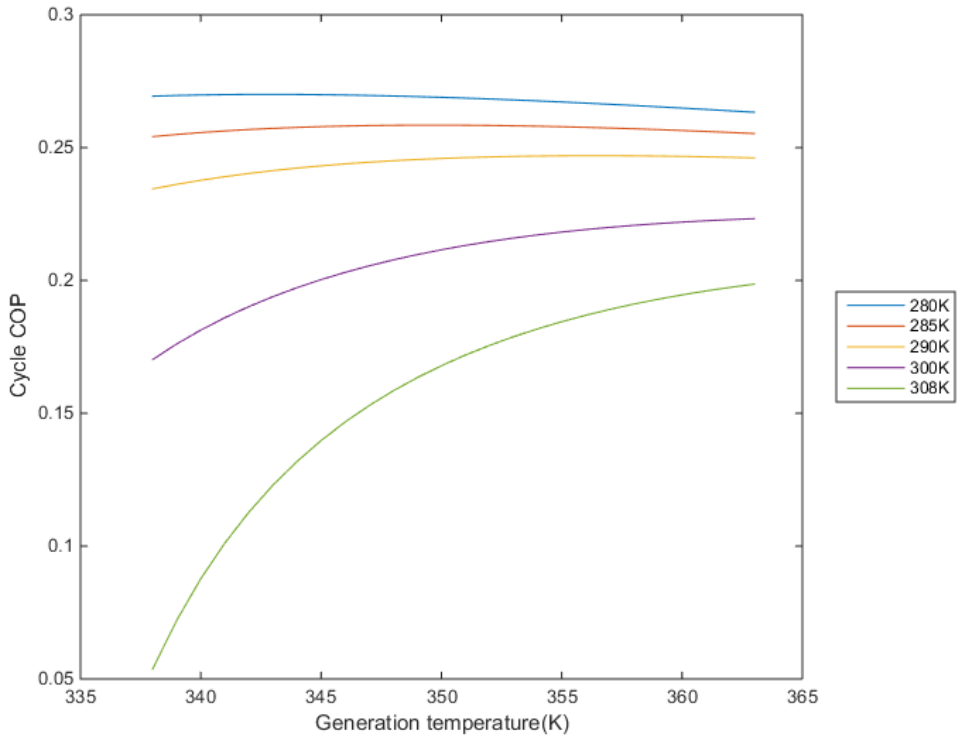

Figure 4.10 - Cycle COP vs Generation temperature for ACF-A20-R134a pair

Figure 4.10 shows the cycle COP as a function of generation temperature and is drawn by varying the value of $T_{a,o}$ (T_1)(temperature at the start of isosteric heating). The plots for these values show that the COP values in for T_1 = 280K decreases as the generation temperature increase while on the contrary for the rest of T_1 values the COP values generally increase as the generation temperature/T_3 increase. Hence, it can be deduced that for smaller values of T_1 small values of T_3 are required for efficient performance while as higher values of T_1 are used T_3 values tend to increase accordingly.

For values of T_1 = 280K, 285K and 290K the maximum COP values were obtained to be 0.27, 0.2585 and 0.2469 respectively at generation temperatures/T_3 of 342-344, 349-350, and 355-358K. The corresponding minimum COPs obtained were 0.2633, 0.2541, and 0.2345 respectively at generation temperature/T_3 value of 363K for T_1 = 280K and T_3 = 338 for T_1 = 285 and 290K. As for T_1= 300 and 308K the maximum attainable COPs were 0.2233, and

0.1986 respectively at generation temperature of 363K. The minimum COP attained for T_1= 300 and 308K were 0.1702 and 0.0537 at T_3 = 338K.

4.3.1.2 Cycle COP vs Generation temperature for Granular AC-R134a pair

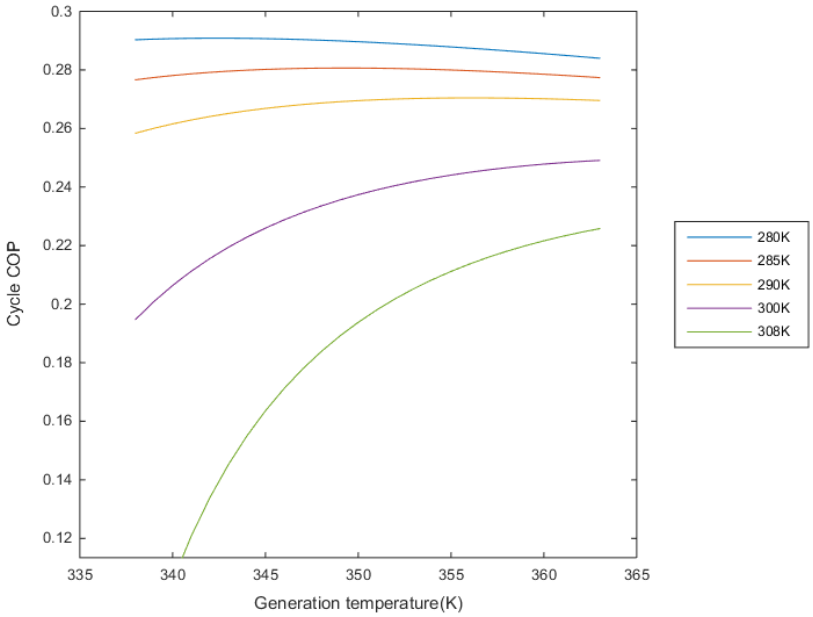

Figure 4.11 - Cycle COP vs Generation temperature for Granular AC-R134a pair

In figure 4.11 it is shown that the COP values for T_1 = 280K decrease as the generation temperature increase while on the contrary for the other T_1 values of the COP values generally show an incremental trend as generation temperature increase. The maximum COP value was recrded at T_1 = 280K. The maximum value of COP is 0.2908 for generation temperatures of 341-344K. At $T_{generation}$ = 363K the minimum COP was recorded at 0.284. At 285K and 290K the maximum COP values were obtained to be 0.2807 and 0.2705 at generation temperature/T_3 of 349 and 356K respectively. The corresponding minimum COPs obtained were 0.2766, and 0.2584 at generation temperature/T_3 value of 338K. As for T_1= 300 and 308K the maximum attainable COPs were 0.2491 and 0.2258 respectively at generation temperature of 363K and the respective minimum COPs were 0.1948 and 0.0657 at T_3 = 338K. The maximum and

minimum values of COP increased as compared to ACA-F20 which was due to the higher value of adsorption capacity.

The similar results of the three pairs in figure 4.9, 4.10 and 4.11 clearly shows how the COP value varies with generation temperature. For an adsorption temperature of 308K, COP increases significantly with an increase in generation temperature. However, variations in COP were found to be negligible.

4.3.1.3 Cycle COP vs Generation temperature for Maxsorb III-R134a pair

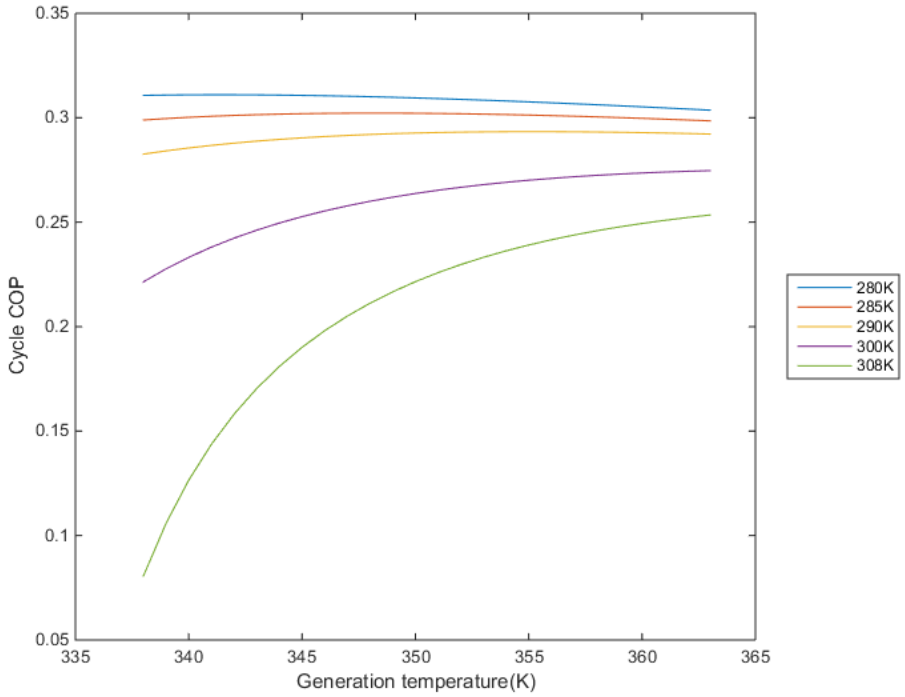

Figure 4.12 - Cycle COP vs Generation temperature for Maxsorb III-R134a pair

Figure 4.12 is plotted for Maxsorb III-R134a pairs and it shows the COP values as a function of generation temperature. For values of T_1 = 280K, 285K and 290K the maximum COP values were obtained to be 0.311, 0.3022 and 0.2934 at generation temperatures/T_3 of 340-343K, 347-349 and 355K respectively. The corresponding minimum COPs for T_1 values of 280 and 285K were 0.3036, 0.2985, at T_3 value of 363 and for T_1 = 290K a minimum COP of 0.2826 was

obtained at 338K. As for T_1= 300 and 308K the maximum attainable COPs were 0.2747, and 0.2535 respectively at generation temperature of 363K and the respective minimum COPs were 0.2215 and 0.08065 at T_3 = 338K. The maximum and minimum values of COP increased as compared to ACA-F20 and granular AC which was due to the higher value of adsorption capacity.

4.3.2 Cycle COP vs Final Desorbed Concentration

4.3.2.1 Cycle COP vs Desorbed Concentration for ACF-A20-R134a pair

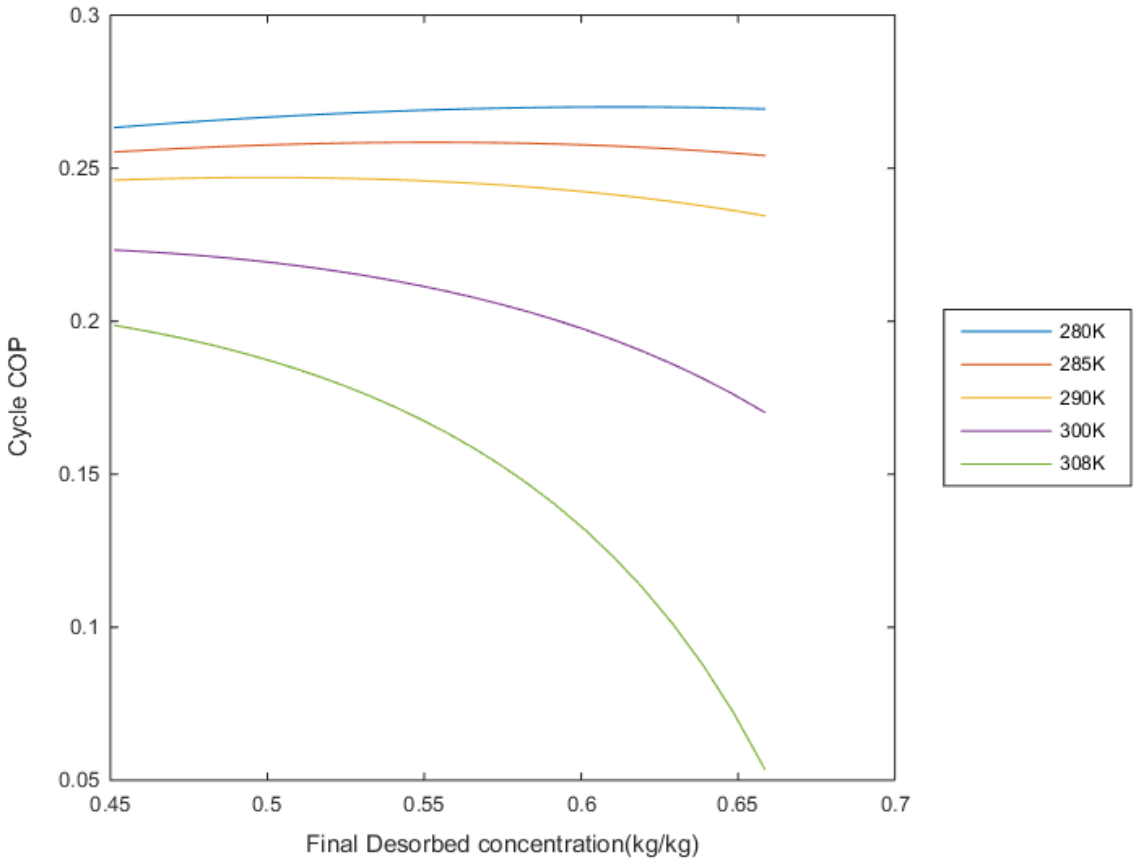

Figure 4.13 - Cycle COP vs Desorbed Concentration for ACF-A20-R134a pair

Figure 4.13 shows the cycle COP as a function of desorbed concentration of the refrigerant for ACF-A20. The plots for values of T_1 = 280K, 285K and 290K show that the highest COP values

can be obtained for final desorbed concentrations of 0.6012-0.6197, 0.549-0.5574 and 0.4866-0.5091 kg.kg^{-1} respectively. For T_1 values of 300K and 308K the COP values decrease as the desorbed concentration increases. This is due to the fact that at higher values of T_1 the maximum COP is obtained at higher desorption temperatures which in turn increase the amount of heat input required for desorption. This results in decreased COP.

As for T_1= 300 and 308K the maximum attainable COPs were obtained at concentration of 0.4514 kg.kg^{-1} and the minimum COPs were obtained at 0.6585 kg.kg^{-1}.

4.3.2.2 Cycle COP vs Desorbed Concentration for Granular AC-R134a pair

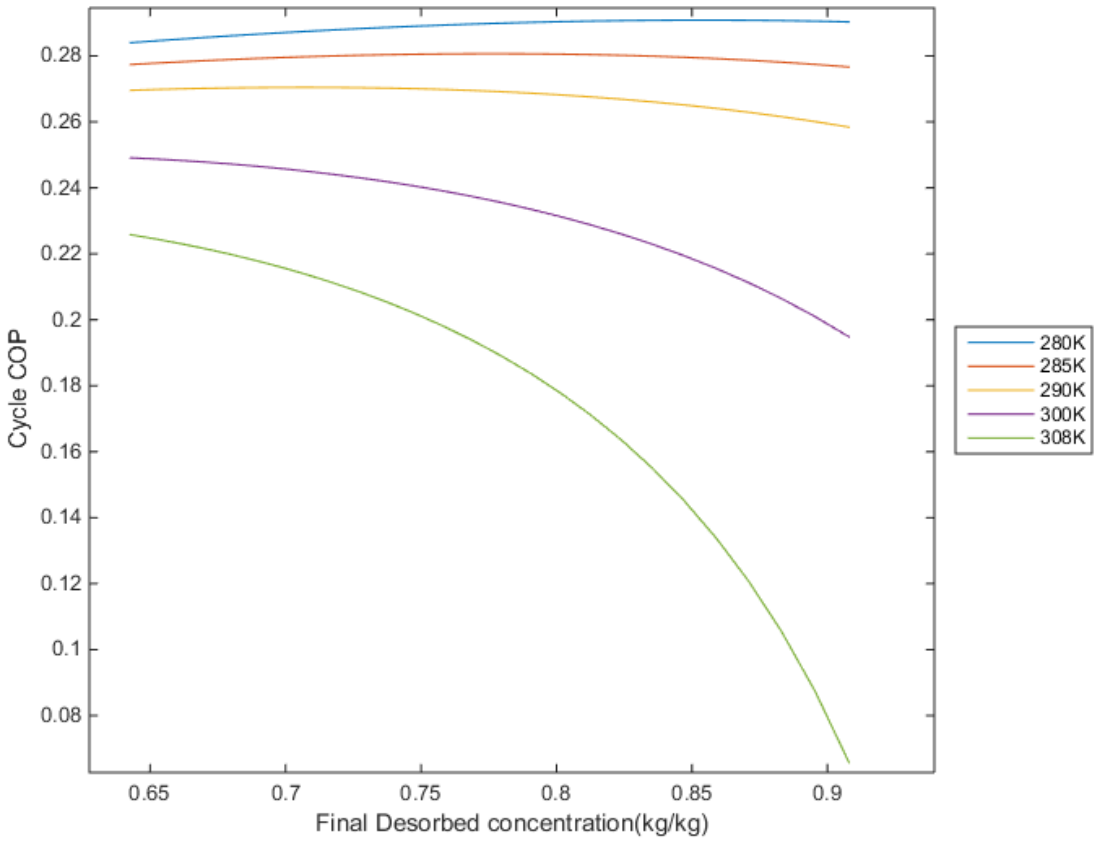

Figure 4.14 - Cycle COP vs Desorbed Concentration for Granular AC-R134a pair

The COP of granular AC versus final desorbed concentration of the refrigerant are depicted in figure 4.14. As in the previous case the plots for value of T_1 = 280K COP increases with increasing amount of the final adsorbate concentration but declines after reaching maximum COP value. For the rest of T_1 values the COP values decrease as the desorbed concentration increases. For values of T_1 = 280K, 285K and 290K the maximum COP values were obtained at final desorption concentrations of 0.8354, 0.7795, 0.7077 kg.kg^{-1}, and the corresponding minimum COPs were obtained at concentration of 0.6427 kg.kg^{-1} for T_1 = 280K, and 0.908 kg.kg^{-1} for T_1 = 285 and 290K. For T_1= 300 and 308K the maximum attainable COPs were obtained at concentration of 0.6427 kg.kg^{-1} and the minimum COPs were obtained at 0.908 kg.kg^{-1}.

4.3.2.3 Cycle COP vs Desorbed Concentration for Maxsorb III-R134a pair

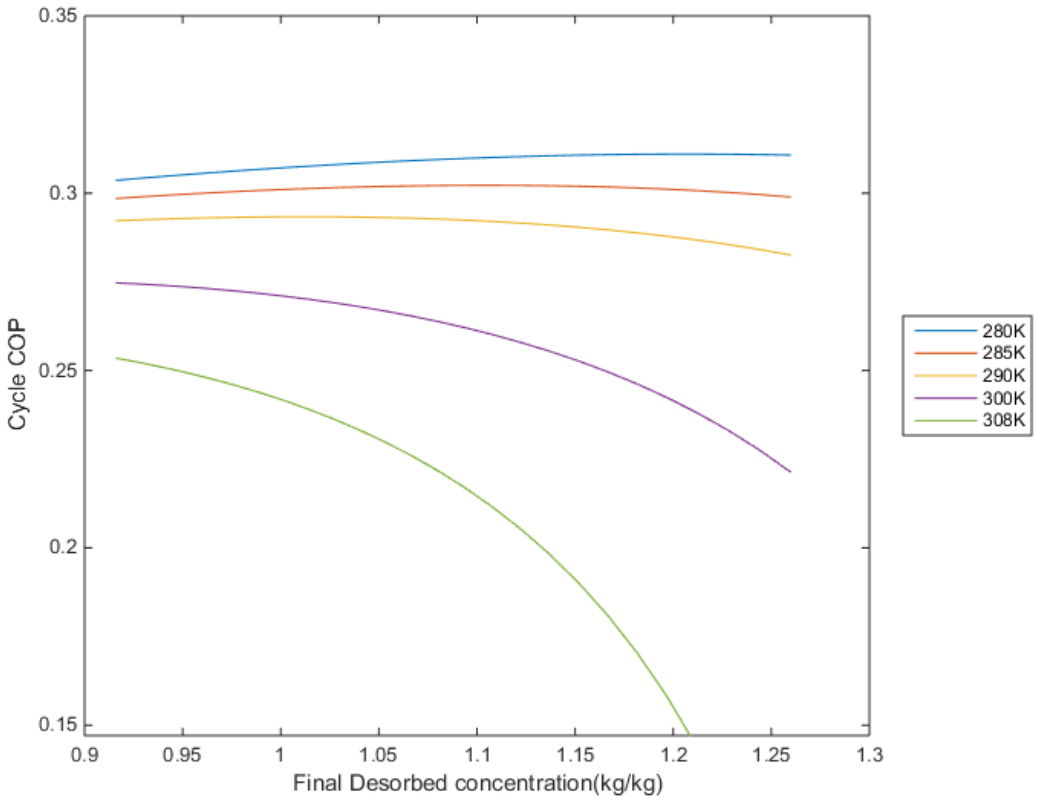

Figure 4.15 - Cycle COP vs Desorbed Concentration for Maxsorb III-R134a pair

The COP of Maxsorb III versus final desorbed concentration of the refrigerant are depicted in figure 4.15. As in the previous case the plots for values of T_1 = 280K, 285K and 290K show that the COP values in this temperature ranges increase as the desorbed concentration increases while the opposite is true for T_1 values of 300K and 308K.

For values of T_1 = 280K, 285K and 290K the maximum COP values were obtained at final desorption concentrations of 1.228, 1.123 and 1.014 kg.kg^{-1} respectively. And the corresponding minimum COPs for these temperature ranges were obtained at a concentration of 0.9163 kg.kg^{-1}. For T_1= 300 and 308K the maximum attainable COPs were obtained at concentration of 0.91363 kg.kg^{-1} and the minimum COPs were obtained at 1.26 kg.kg^{-1}.

4.3.3 SCP vs Generation temperature

4.3.3.1 SCP vs Generation temperature for ACF-A20-R134a pair

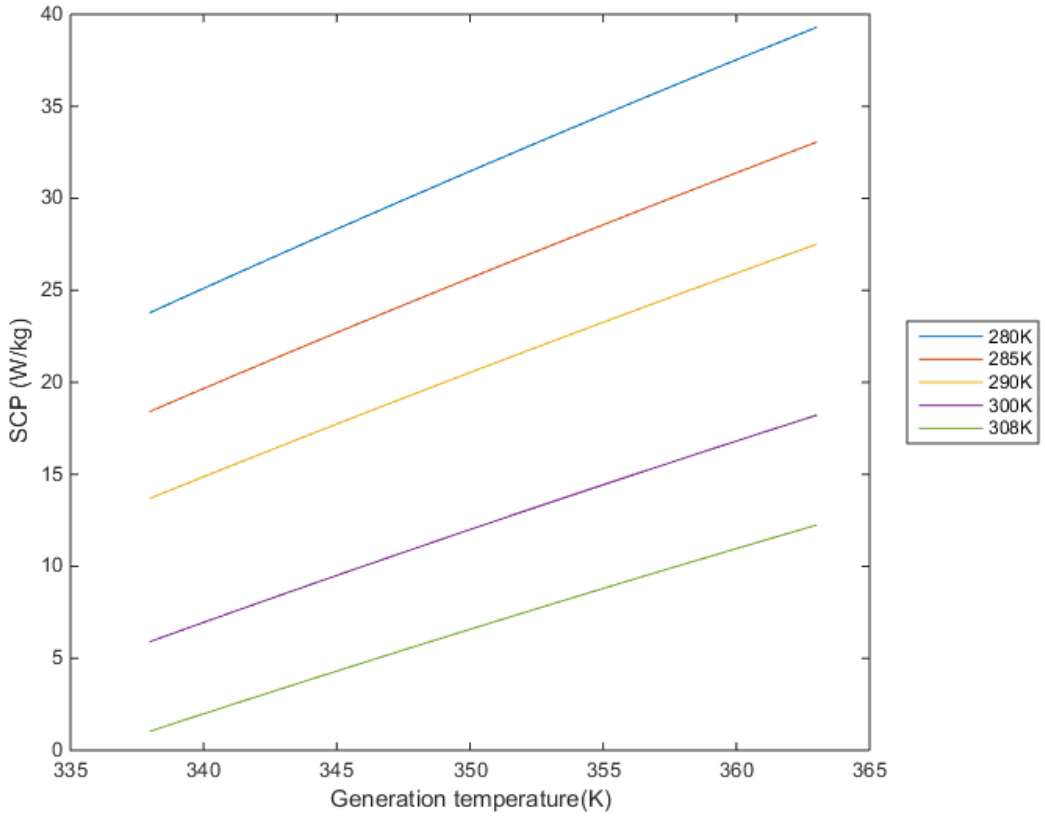

Figure 4.16 - SCP vs Generation temperature for ACF-A20-R134a pair

Another performance indicator is the specific cooling power. This determines the size of the adsorption cooling system. Here, in the same manner as the previous plots, the SCP is drawn against generation temperature for different values of T_1 in figure 4.16. Unlike the previous diagrams the SCP increases as the generation temperature increases for all values of T_1. The maximum values of SCP obtained are 39.29, 33.05, 27.5, 18.21, 12.24 W/kg for T_1 values of 280, 285, 290, 300, and 308K respectively. This values were obtained at maximum generation temperature of 363K (90°C). Correspondingly, the minimum values of SCP for T_1 values of 280, 285, 290, 300, and 308K were found to be 23.8, 18.43, 13.7, 5.917, and 1.043 W/kg at a generation temperature of 338K.

4.3.3.2 SCP vs Generation temperature for Granular AC-R134a pair

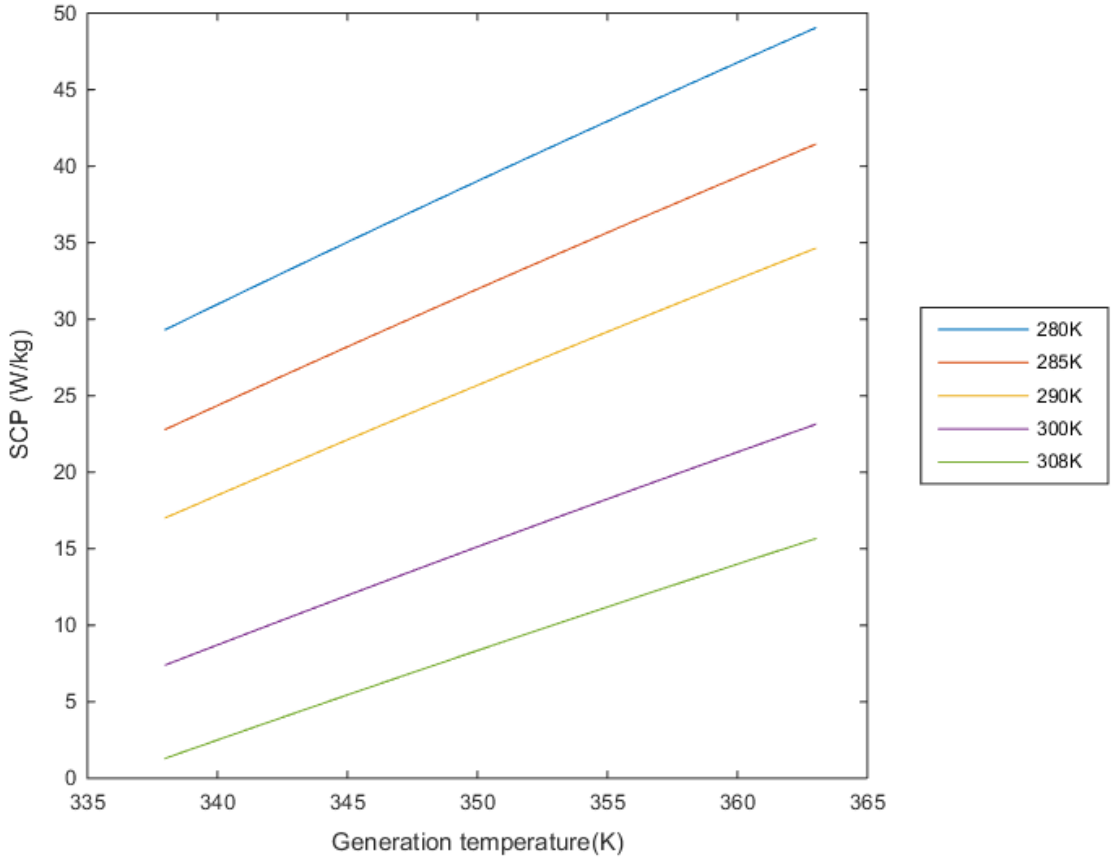

Figure 4.17 - SCP vs Generation temperature for granular AC-R134a pair

Granular AC-R134a pair has higher SCP value as compared to ACF-A20-R134a pair. Shown in figure 4.17, for all values of T_1 the SCP value tended to increase with increasing values of T3/generation temperature. The maximum values of SCP obtained were 49.03, 41.43, 34.63, 23.13, 15.66 W/kg for T_1 values of 280, 285, 290, 300, and 308K respectively. This values were obtained at maximum generation temperature of 363K (90°C). Correspondingly, the minimum values of SCP for T_1 values of 280, 285, 290, 300, and 308K were found to be 29.33, 22.8, 17.02, 7.408, 1.315 W/kg at a generation temperature of 338K.

4.3.3.3 SCP vs Generation temperature for Maxsorb III-R134a pair

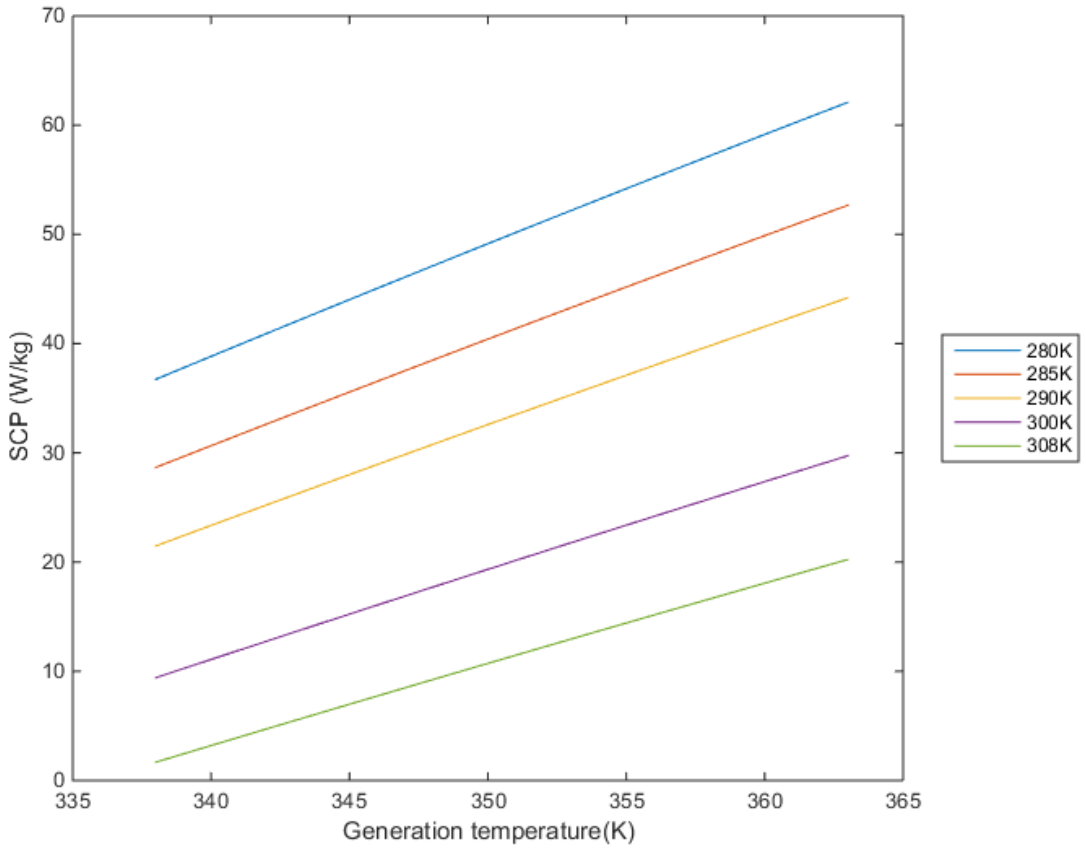

Figure 4.18 - SCP vs Generation temperature for Maxsorb III-R134a pair

The SCP value indicates how much cooling power can be delivered by the adsorbate pair per kg of adsorbent. The SCP for Maxsorb III-R134a pairs increases as the generation temperature increases for all values of T_1 as evidenced from figure 4.18. The maximum values of SCP obtained are 62.09, 52.67, 44.19, 29.73 and 20.23W/kg for T_1 values of 280, 285, 290, 300, and 308K respectively. This values were obtained at maximum generation temperature of 363K (90°C). Correspondingly, the minimum values of SCP for T_1 values of 280, 285, 290, 300, and 308K were found to be 36.73, 28.66, 21.48, 9.409 and 1.677 W/kg at a generation temperature of 338K. In solar adsorption systems, both COP and SCP have to be clearly determined and optimized to have and efficient and effective solar adsorption system.

4.3.4 Cycle COP vs SCP

4.3.4.1 Cycle COP vs SCP for ACF-A20-R134a pair

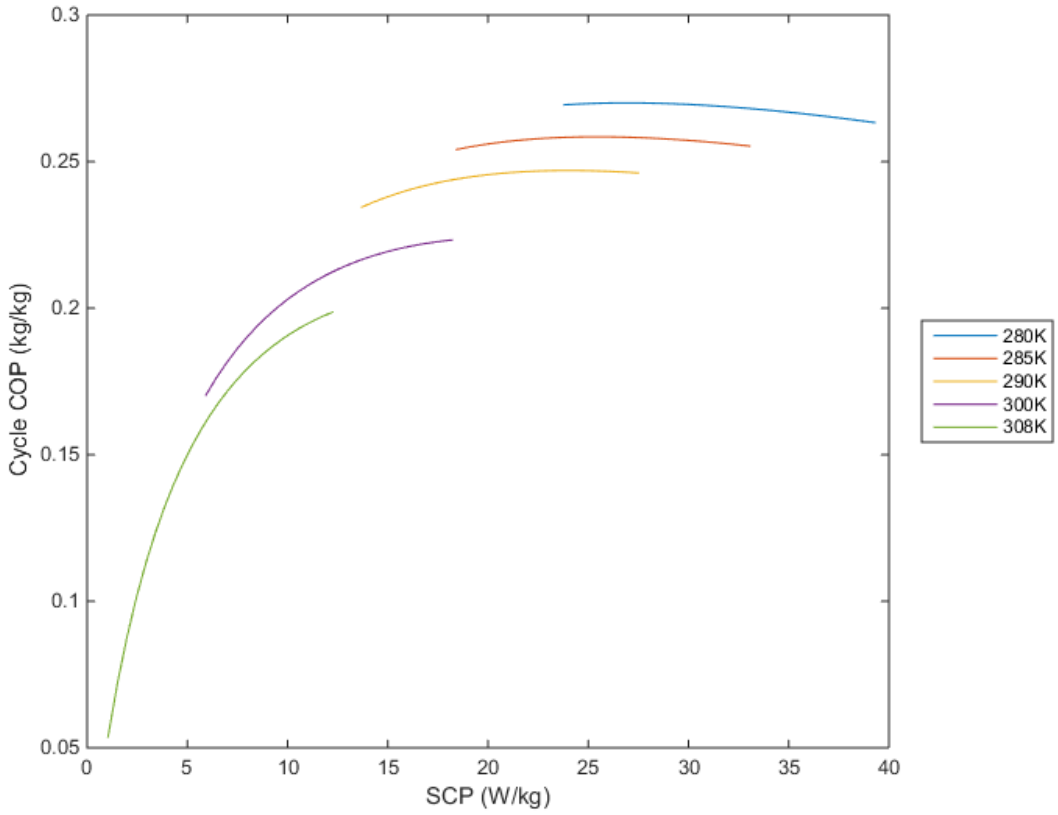

Figure 4.19 - Cycle COP vs SCP for ACF-A20-R134a pair

Plot of cycle COP against SCP shows for ACF-A20-R134a is given in figure 4.19. For values of T_1 = 280, 285, and 290K the COP will be highest for SCP values of 26.4-27.69, 25.05-25.67 and 23.27–24.87W/kg. When it comes to T_1 values of 300 and 308K the SCP values that yield the highest value of cycle COP are 18.21 and 12.24 W/kg. Therefore, from the graph it is evident that if operating in the temperature ranges of T_1=280, 285 and 290K getting higher values of COP decreases the potential of obtaining higher SCP values but the opposite is true for T_1 = 300 and 308K.

4.3.4.2 Cycle COP vs SCP for Granular AC-R134a pair

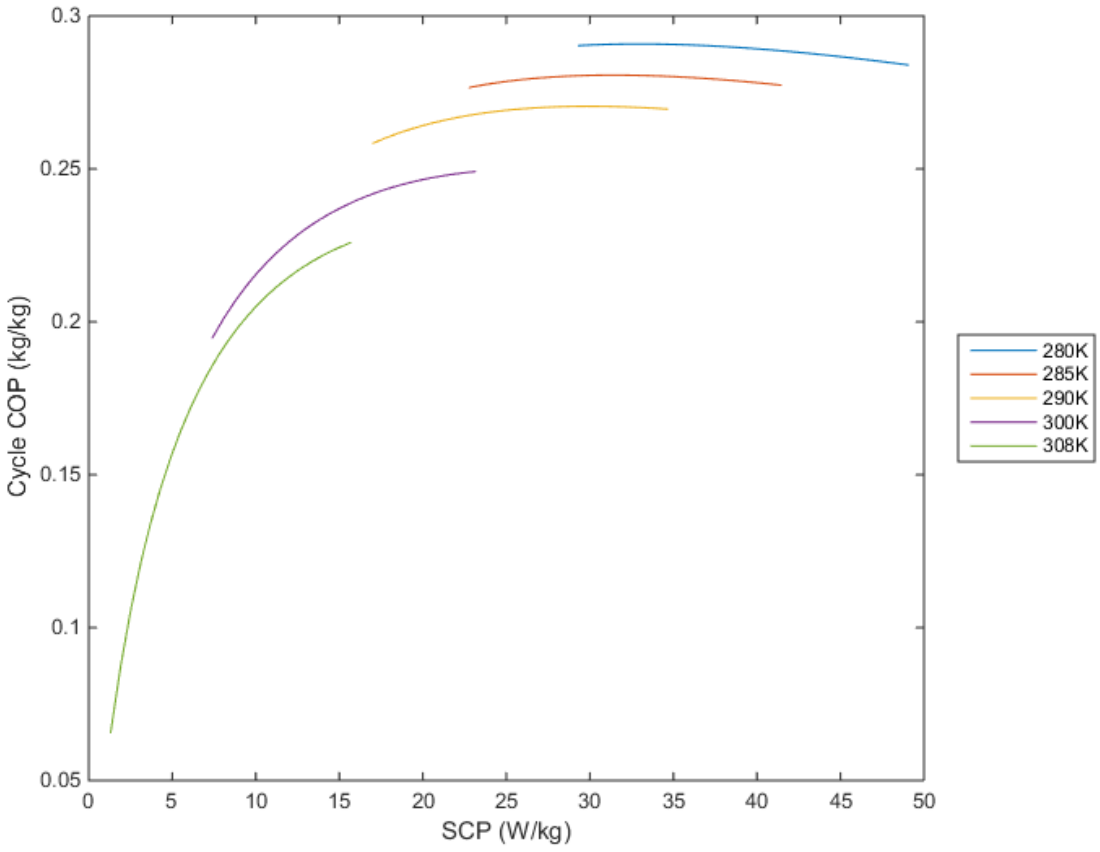

Figure 4.20 - Cycle COP vs SCP for Granular AC-R134a pair

In figure 4.20, plot of cycle COP against SCP is given for Granular AC-R134a pairs. For T_1 = 280, 285, and 290K the COP will be highest for SCP values of 31.79-33.42, 31.22 and 29.87W/kg respectively. When it comes to T_1 values of 300 and 308K the SCP values that yield the highest value of cycle COP are 23.13 and 15.66 W/kg. Therefore, from the graph it is evident that if operating in the temperature ranges of T_1=280K getting higher values of COP decreases the potential of obtaining higher SCP values but the opposite is true for the rest of T_1 values.

4.3.4.3 Cycle COP vs SCP for Maxsorb III-R134a pair

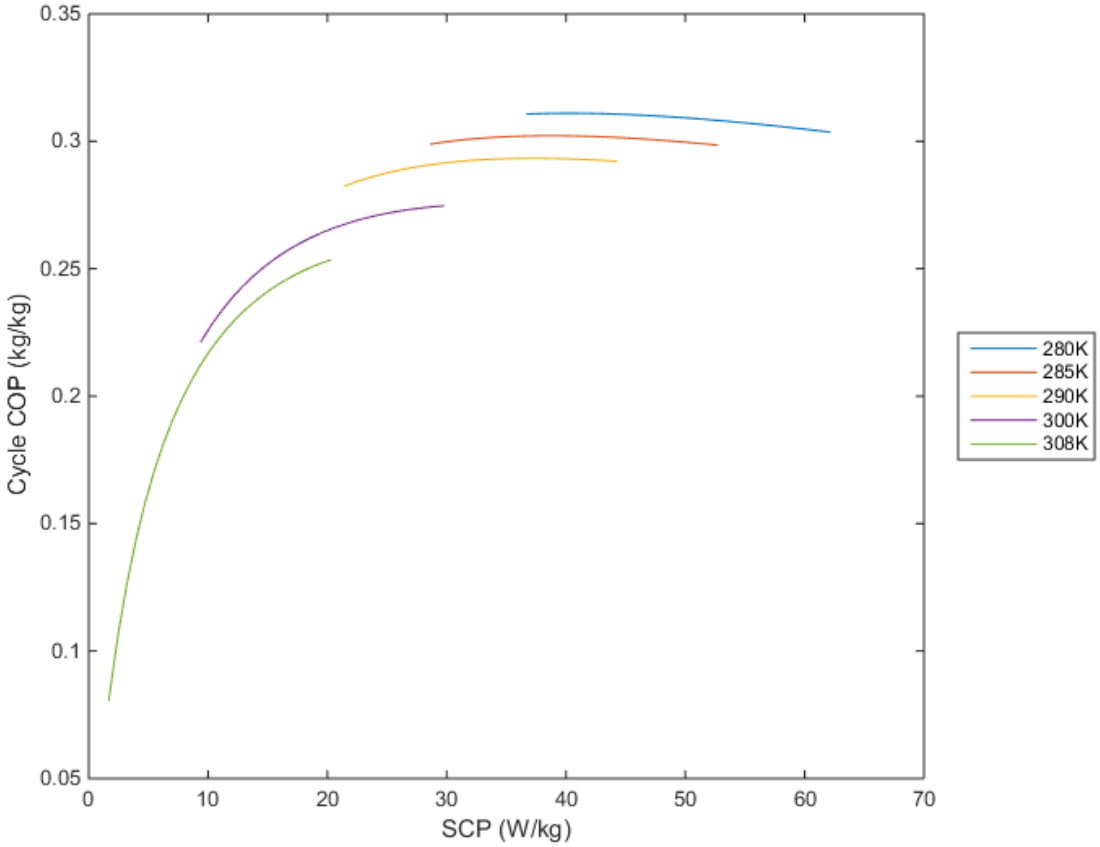

Figure 4.21 - Cycle COP vs SCP for Maxsorb III-R134a pair

The relationship between cycle COP and SCP is important as it dictates our operating conditions. From figure 4.21, it can be observed that as the SCP increases for T_1 = 280, 285,

and 290K the COP shows a slight decrement in value for Maxsorb III-R134a pairs. Hence, if there is a need to operate in these ranges higher COP values can only be obtained at the expense of SCP. On the contrary, for T_1 values of 300 and 308K, as the SCP values increase, higher COP values can be obtained.

Therefore, from the graph it is evident that if operating in the temperature ranges of T_1=280, 285 and 290K getting higher values of COP decreases the potential of obtaining higher SCP values. The opposite is true for T_1 = 300 and 308K as higher SCP values can only be obtained if the COP values are also high. Hence, it is up to the designer to choose which operating conditions are favorable as per the cooling requirement. Figures 4.19, 4.20 and 4.21 clearly show how compactness of the system (higher SCP) influences COP. Additionally, starting the heating process at a lower adsorption outlet temperature significantly increases the performance if supported by higher SCP.

4.3.5 Monthly Solar COP

4.3.5.1 Monthly Solar COP for ACF-A20-R134a pair

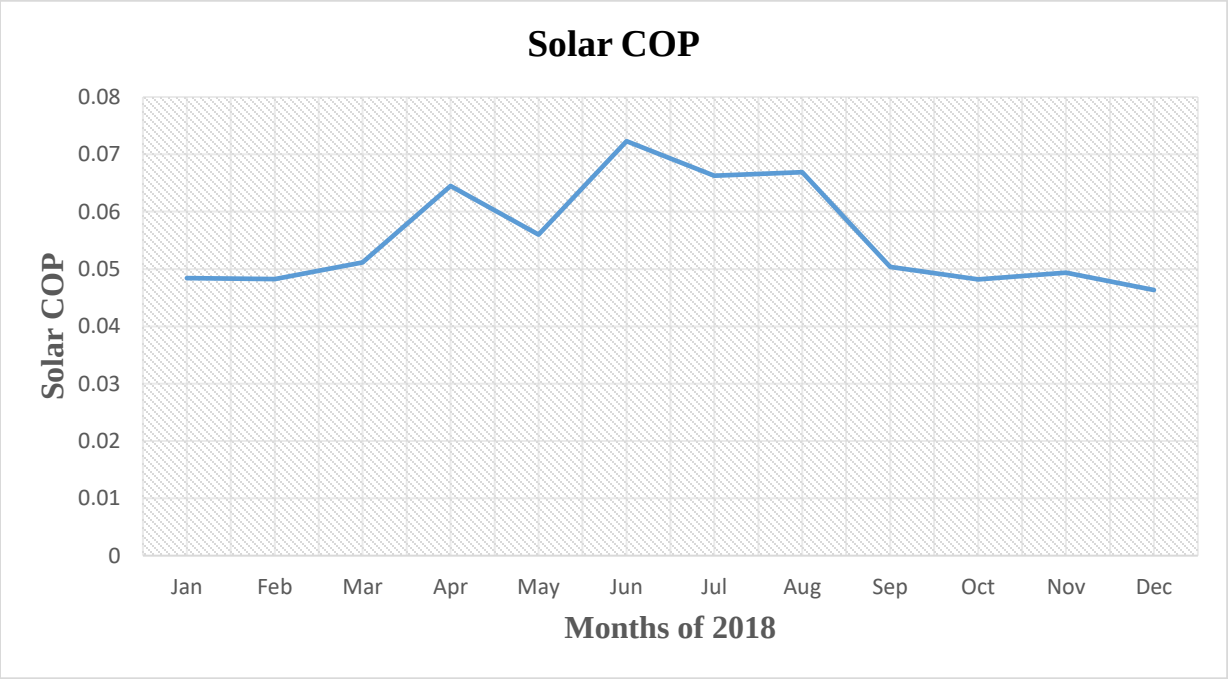

Figure 4.22 - Monthly Solar COP for ACF-A20-R134a pair

The solar COP for the first six months of 2018G.C are shown in figure 4.22. From the plot, the minimum solar COP was recorded in the month of December with a value of 0.0463. The low solar COP value was due to the high value of solar radiation in the specific month as compared to the cooling effect required. The COP was the highest for the month of June which was about 0.072. This value indicates that the radiation in this specific month is closely matched with the cooling load of the refrigeration/chiller system.

From the beginning of the year the solar COP increases and hits a peak value 0.064 in April which is the highest value for the first 4 months of the year. From that point on the COP values suddenly show a sharp decrement to 0.056 in May before increasing again to the maximum COP value. After achieving the highest COP value in June it steadily decreases since the amount of heat input with the radiation energy increases showing an overall decreasing trend in the value of the solar COP.

4.3.5.2 Monthly Solar COP for Granular AC-R134a pair

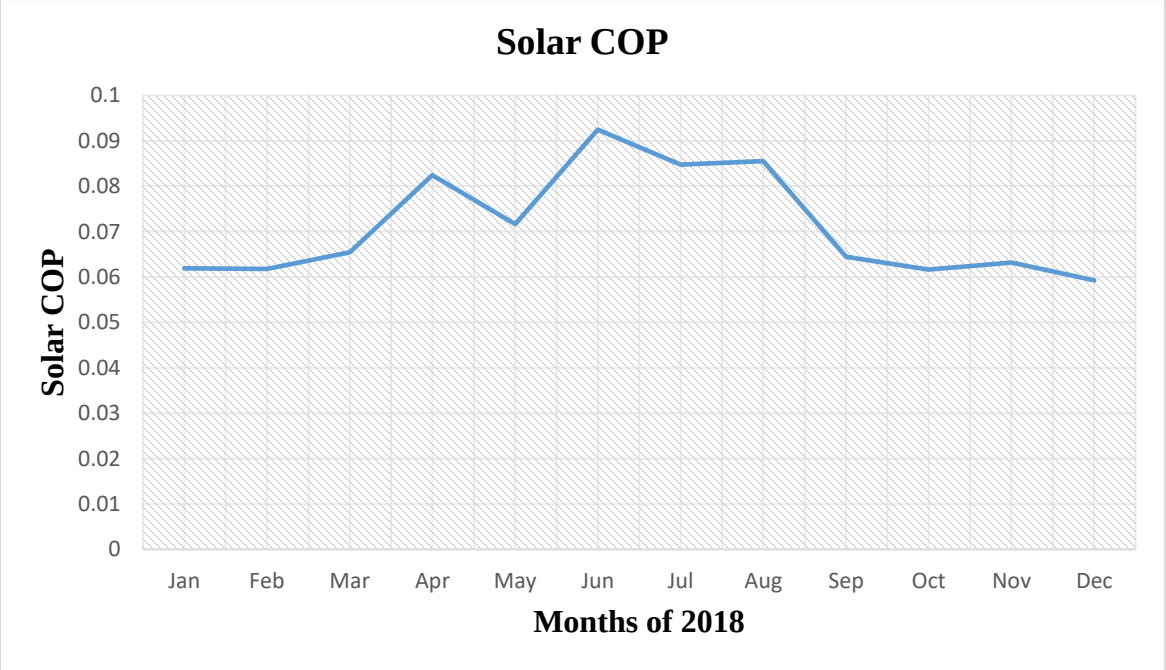

Figure 4.23 - Monthly Solar COP for Granular AC-R134a pair

The solar COP values of the first six months of 2018 G,C are shown in figure 4.23. The minimum solar COP was recorded in the month of December with a value of 0.059. The COP was the highest for the month of June which was about 0.092. From the beginning of 2019 the solar COP increases and hits a peak value 0.082 in April which is the highest value for the first 4 months of the year. From that point on the COP values suddenly dips to 0.0716 in May before increasing again to the maximum COP value. As observed in the previous case, the solar COP here also shows a decreasing trend after June showing a dramatic decrease going from August to September and then steadily decreasing to a minimum solar COP value in December.

4.3.5.3 Monthly Solar COP for Maxsorb III-R134a pair

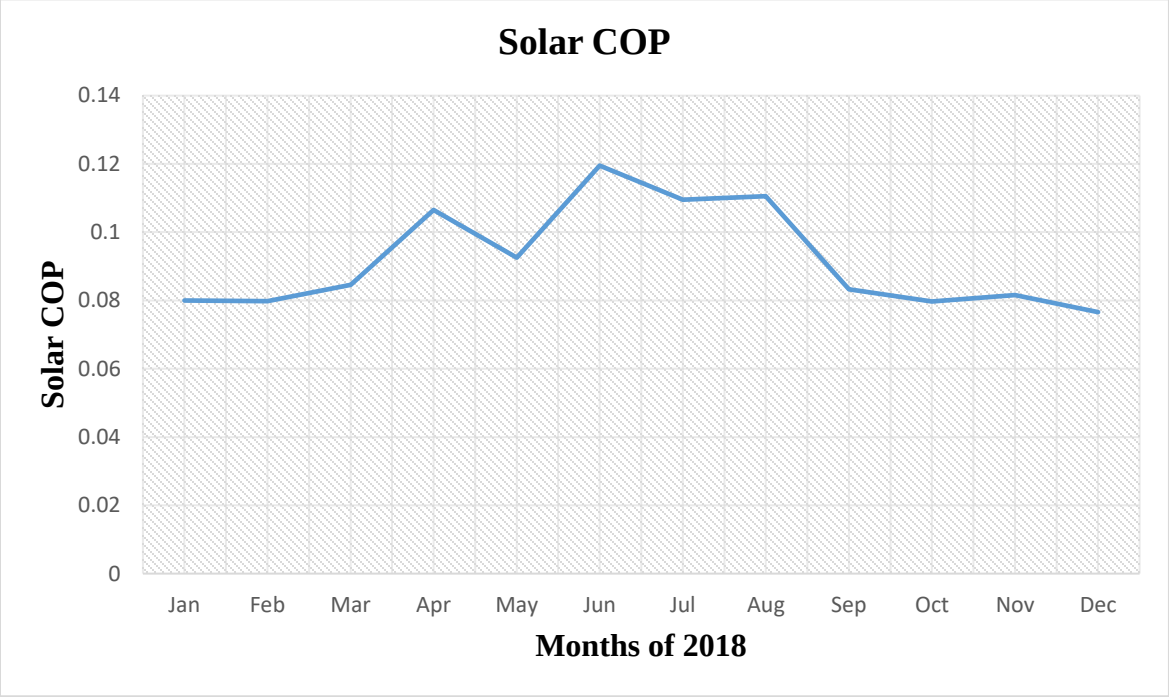

Figure 4.24 - Monthly Solar COP for Maxsorb III-R134a pair

The solar COP values for Maxsorb III in the first six months of 2018 are shown above in figure 4.24. The minimum solar COP was recorded in the month of December with a value of 0.076. The COP was the highest for the month of June which was about 0.119. From the beginning of 2018 the solar COP increases and hits a peak value 0.106 in April which is the highest value

for the first 4 months of the year. From that point on the COP values suddenly dips to 0.0925 in May before increasing again to the maximum COP value.

4.3.6 Optimization the generation temperature

In all the activated carbon and R134a pairs, the maximum COP was obtained at an initial bed temperature, $T_{a,i}$ = 280K. However, the optimum generation temperature is not fixed. In order to obtain the optimum value of the generation temperature the SCP and COP values were drawn against varying generation temperature and a point of intersection was taken to be the optimum point. For the three pairs taken into consideration this is shown as follows.

4.3.6.1 Optimization the generation temperature for ACF-A20-R134a pairs

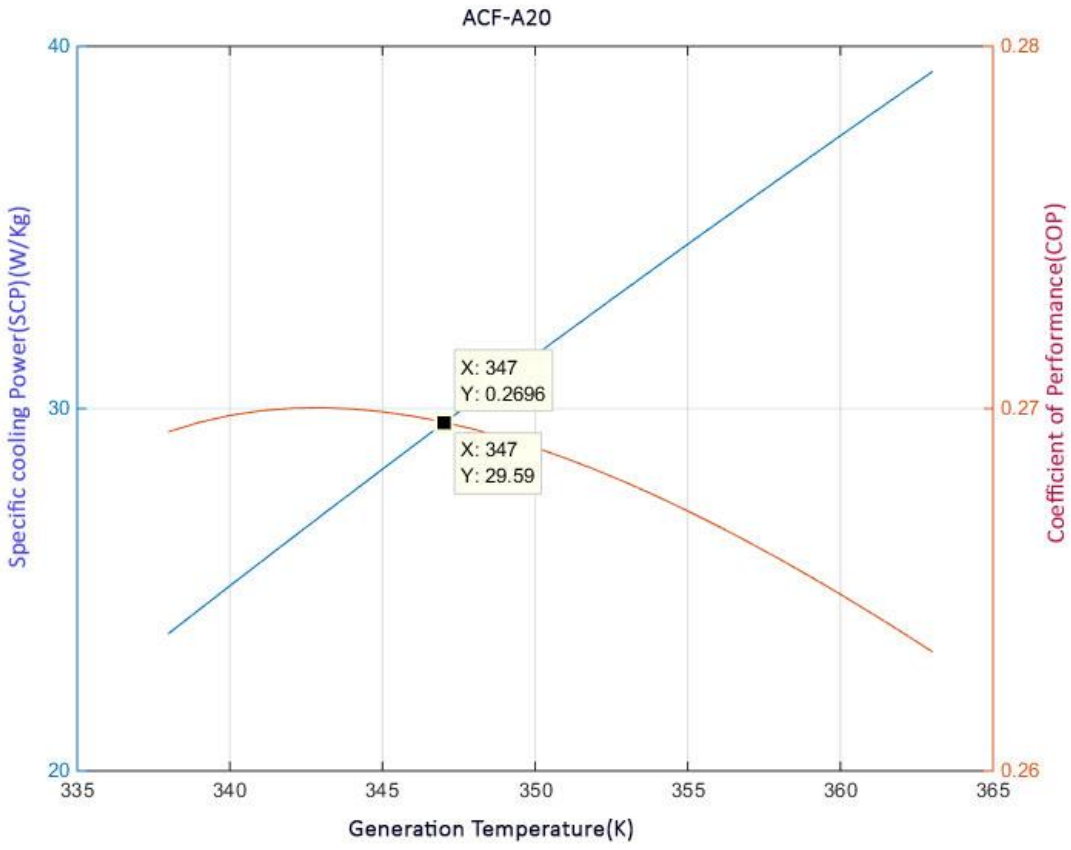

Figure 4.25 - Optimum generation temperature for ACF-A20-R134a pairs

Graph 4.25 shows the optimum generation temperature for ACF-A20-R134a pairs at bed temperature of 280K. From the plot the point of intersection of the SCP and COP curves drawn against generation temperature was selected as optimum point of operation. Hence, for the intersection point shows that a generation temperature of 347K is optimum. At this point the COP and SCP values were 0.2696 and 29.59W/kg.

4.3.6.2 Optimization the generation temperature for Granular AC-R134a pairs

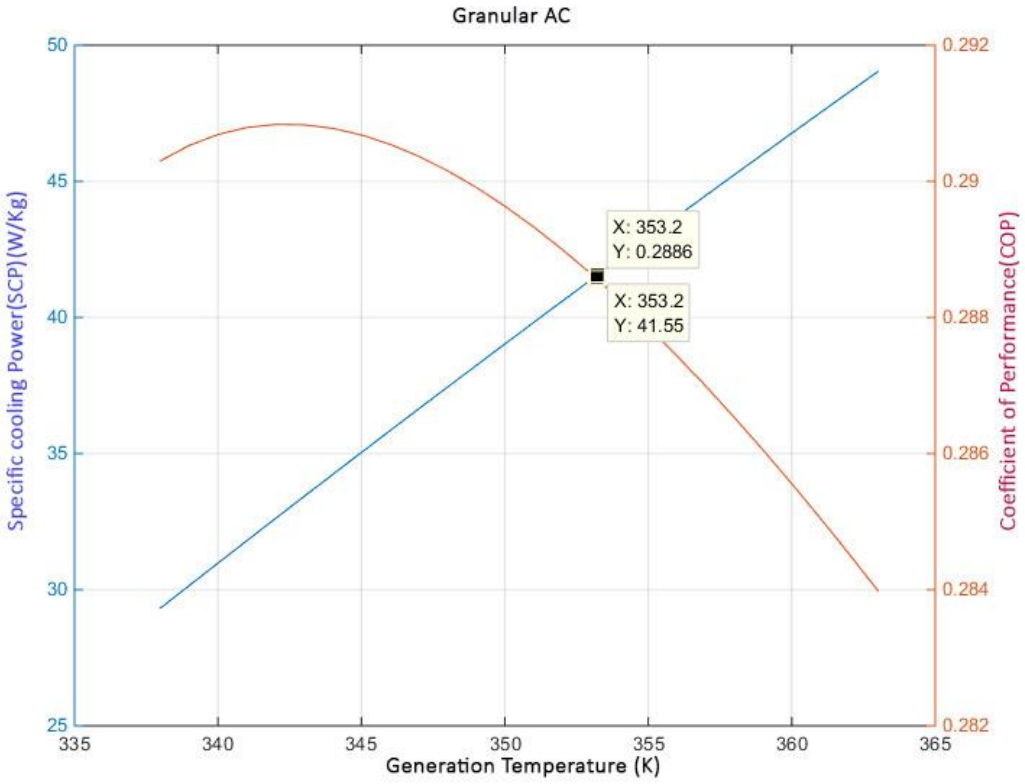

Figure 4.26 - Optimum generation temperature for Granular AC-R134a pairs

In the above figure 4.26, the plot of COP and SCP against generation temperature was done for the initial bed temperature of $T_{a,i}$ = 280K. The plot of the curves intersects as in the previous case, giving the optimum generation temperature. Hence, from the above plot, the two curves intersected at generation temperature of 353.2K. The SCP and COP values that give this optimum generation temperature were found to be 0.2886 and 41.55W/kg respectively

4.3.6.3 Optimization the generation temperature for Maxsorb III-R134a pairs

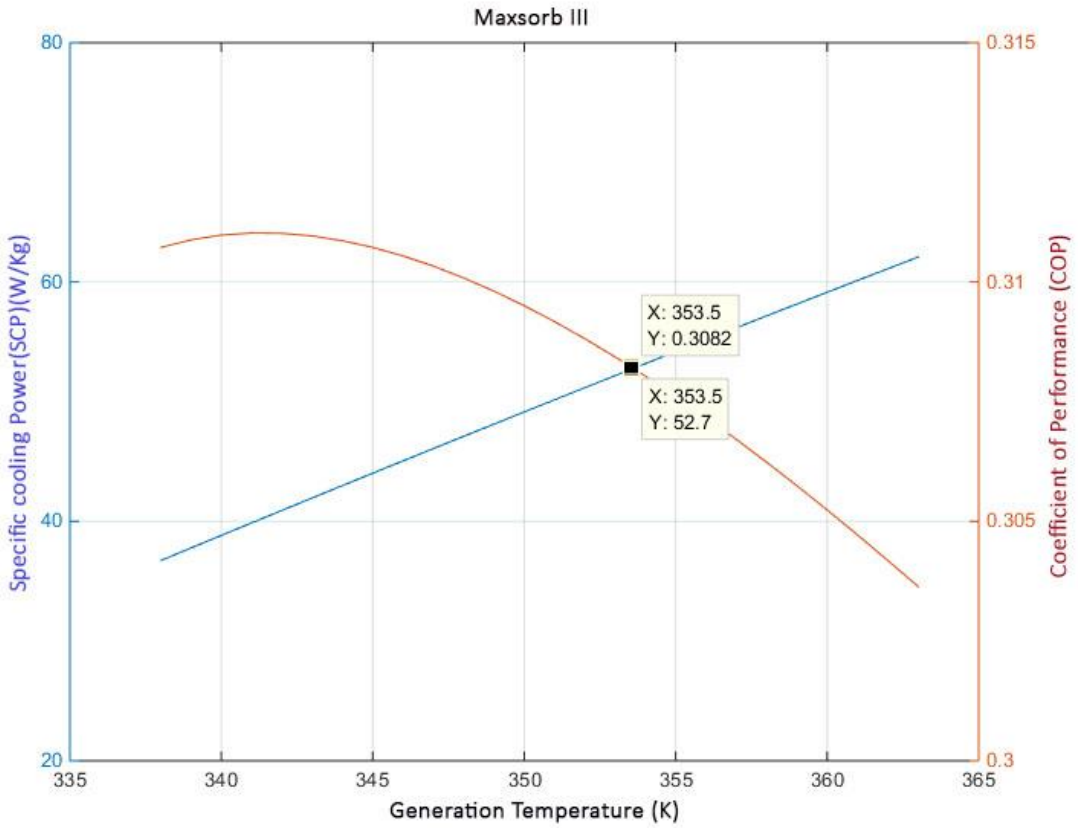

Figure 4.27 - Optimum generation temperature for Maxsorb III-R134a pairs

In figure 4.27, the plot of SCP and COP is shown in order to determine the most plausible generation temperature at initial bed temperature of 280K. Hence, the plot of COP and SCP against generation temperature was taken and at the intersection point an optimum generation temperature

of 353.5K was found. At this temperature, the optimum point yielding COP and SCP values were found to be 0.3082 and 52.7W/kg respectively.

4.3.7 Comparative Analysis and Validation of results

The results of the simulation revealed COP and SCP values of the adsorption refrigeration for the three activated carbon-R134a pairs increase as the surface area of the activated carbon increases. Hence, Maxsorb III possesses the highest value of COP and SCP. However, the difference in the COP values is not that much appreciable since marginal differences were observed. This indicated that higher surface area (which is required for high adsorption capacity) does not necessarily yield higher COP. As for SCP values, marked differences are observed in that Maxsorb III gives the highest specific cooling power (SCP) at a value of 62.09 W/kg while ACF-A20 and Granular AC have values of 39.29 and 49.03W/kg. Therefore, it can be concluded that for the purpose of refrigeration, if a designer aims at achieving higher SCP values, it is preferable to use Maxsorb III as the adsorbent.

In adsorption refrigeration systems, higher COP values are associated with high adsorption capacities. This is reflected in the results of the simulation. As initial bed temperatures are increased COP values tend to decrease with values of refrigerant concentration decreasing in the same manner. This indicates that as the amount of desorbed refrigerant increases at the end of the desorption process, the COP values increase as well.

From the result of SCP it can be concluded that for the three adsorbents taken into consideration, the highest COP is observed when SCP decreases for T_1 values of 280, 285 and 290K and vice versa for 300 and 308K. Additionally, it is to be concluded that SCP values are dependent on surface area and other physical properties of the adsorbent unlike that of COP results obtained.

Another outcome of the paper is the solar COP. The solar COP is affected by the solar radiation. This value was the highest for Maxsorb III-R134a pairs with solar COP value of 0.119. This is a strong indication to use Maxsorb III in refrigeration applications since it has the highest COP, and SCP values.

4.3.7.1 Validation

The results of this thesis paper were compared with different results obtained by other researchers. K. Habib et. al., (**K Habib, et. al, 2013**) carried out research with Maxsorb III-R134a pairs using two stage cycle and obtained COP values of 0.3 similar to the one obtained in this paper. In this research work, the source of heat is low grade heat instead of direct solar heating.

K. Habib et. al., (**K Habib, et. al, 2013**) studied the performance of three adsorption systems for Kuala Lumpur climate conditions. These systems are silica-gel water, ACF-ethanol and AC-methanol. silica gel water system has the highest value of COP which is around 0.5 followed by the COP values of ACF-ethanol and AC-methanol systems. But when the heat source temperature is more than 70 °C, the COP of ACF-ethanol system reaches up to around 0.55.

Tamainot-Telto et. al. (**Tamainot-Telto et. al., 2009**) studied 26 activated carbon-ammonia pairs for single, two-bed and infinite bed systems. Considering a two-bed cycle, the best thermal performances based on power density were obtained with the monolithic carbon KOH-AC. With driving temperature of 100 °C the cooling production was about 66 MJ/m^3 with 0.45 COP and 151 MJ/m^3 with 0.61 COP for ice making and air conditioning, respectively. The heating production was about 236 MJ/m3 with COP of 1.5.

El-Sharkawy et al. (**El-Sharkawy et. al, 2009**) studied the adsorption of methanol onto carbon based adsorbents namely Maxsorb III and Tsurumi. In this study, the change of SCP and COP with regeneration temperatures for Maxsorb III/methanol, activated charcoal/methanol, LH/methanol, DEG/methanol and AC-35/methanol pairs was studied. The maximum COP was 0.78 with Maxsorb III/methanol at regeneration temperature of 90 °C.

Though higher COPs have been achieved using multiple bed systems, the proposed system with maximum COP of 0.311 and SCP of 62.09 W/Kg in this paper is a simple solar adsorption refrigeration system. Hence, the simple attribute of this cooling system makes it suitable to be manufactured locally.

Chapter 5
Conclusion

In this research paper, the performance of three types of activated carbon utilizing R134a as refrigerant has been studied and reported. The three types of activated carbon are ACF-A20, granular AC and Maxsorb III. These materials have varying properties and characteristics which needed thorough analysis for refrigeration/cooling applications. The operating conditions selected for analysis were $P_{evaporator}$ = 270kPa, $P_{condenser}$ = 600kPa based on the justifications presented in the results and discussions section. The initial exit temperature refrigerant from the bed was varied for different values of T_1 = 280,285,290,300 and 308K and for different generation temperatures of 338 up to 363 were used to analyze the performance of the adsorption pairs.

For adsorption pair ACF-A20-R134a, the maximum COP obtained was 0.27 at T_1 value of 280K and generation temperature of 342-344K while the minimum COP was observed at T_1 value of 308 with a value of 0.0537. The SCP was analyzed for a cycle time of 5800seconds and at T_1=280K maximum SCP of 39.29 W/kg was observed and a minimum value of 1.043W/kg was obtained at T_1 = 308K. Under the aforementioned operating conditions maximum solar COP was 0.072 in the month of June 2018 and minimum solar COP was recorded for December 2018 with a value of 0.0463.

The second pair to be analyzed was granular AC-R134a pair. Due to the higher value of adsorption capacity the COP and SCP values of this adsorption pair were found to be higher as well. As such, the maximum COP obtained was 0.2908at T_1 value of 280K and generation temperature of 341-344K while the minimum COP was observed at T_1 value of 308 with a value of 0.0657. The SCP was analyzed for a cycle time of 5800seconds and at T_1=280K, maximum SCP of 49.03W/kg was observed and a minimum value of 1.315W/kg was obtained at T_1 = 308K. Maximum solar COP obtained was 0.092 for the month of June 2018 and minimum solar COP was observed for December 2018 with a value of 0.059.

The third and final adsorption pair was the Maxsorb III-R134a pair. As the name implies this variant of activated carbon has the highest adsorption capacity as compared to the rest of the adsorbents. Hence the highest COP and SCP values were obtained for this type of activated

carbon. For T_1 value of 280K the maximum COP of 0.311 were obtained and minimum COP value of 0.0806 was obtained for initial desorption temperature T_1 = 308K. Under the same conditions, at T_1 =280K a maximum SCP value of 62.09 W/kg was recorded for generation temperature of 363K and minimum value of 1.677W/kg was obtained for T_1 value of 308K under a generation temperature of 338K. Maximum Solar COP was 0.119 and minimum value of solar COP was 0.076 for the months of June and December respectively.

The optimization of the generation temperature was also evaluated and it shows that operating at optimal value of generation temperature decreases the COP and SCP values from their maximum points. Hence for ACF-A20 the optimum generation temperature is 347K at COP and SCP values of 0.2696 and 29.59 W/kg. For granular AC optimum value is 353.2 at COP of 0.2886 and SCP of 41.55 W/kg. Maxsorb III has an optimum point of 353.5 at COP of 0.3082 and 52.7 W/kg.

The economic analysis for the most efficient activated carbon type, Maxsorb III, was carried out. As such, the net present value of -3375.1 ETB, annual net worth of -1,109.63 ETB and an internal rate of return value of -23% were found. The fact that these values are negative normally implies that the investment is uneconomical but in reality the actual value of the equipment lies in giving cooling service after an initial investment or purchasing value of 4,875 ETB is spent on it.

The value of COP and SCP obtained for these types of adsorption pairs is a helpful tool in providing essential information for designers and organizations wishing to construct the refrigeration system and disseminate it to remote locations which are currently out of the main grid system. Other researchers and implementers can take valuable information not only for design purposes but to choose the optimum operating conditions that can best serve their goals.

Therefore, the information provided in this thesis paper is based on simulation test of the operating conditions mentioned above and actual testing is imperative to validate the results fully. However, the results presented are indicative of the performance abilities of the three types of adsorbent pairs and can provide preliminary information.

Recommendations for Future Work

Adsorption refrigeration systems find applications in areas of the world that are hugely endowed with solar energy. In countries such as Ethiopia, the opportunity of using solar energy potential presents itself in energy application for various purposes, one of them being solar adsorption refrigeration.

As this study is concerned on the performance analysis of activated carbon-R134a pairs, it puts emphasis on the importance of researching and investing in adsorption refrigeration systems for off-grid areas of Ethiopia which can greatly benefit from solar powered appliances. Hence, it is recommended that rigorous investment and research initiatives must be promoted in this specific area as it benefits the livelihoods of off-grid areas engaged in commercial cattle herding and fishery since the technology enhances the quality of their product on the market.

Secondly, since this research work is based on simulation analysis of three types of activated carbon-R134a adsorbate-adsorbent pairs, further experimental work should be done to fully validate the results obtained. Therefore, individual and organizational research entities should be heavily involved and implement the extra research work needed in order to kick start development and dissemination of solar adsorption refrigeration systems that benefits rural and off-grid locations of Ethiopia.

References

1. Mahmoud B. Elsheniti, Osama A. Elsamni, Raya K. Al-dadah, Saad Mahmoud, Eman Elsayed and Khaled Saleh, *Adsorption Refrigeration Technologies*,. Intechopen., June 2018
2. Ruzhu Wang, Liwei Wang and Jingyi Wu., *Adsorption refrigeration technology: Theory and application***,** SJTU., John Wiley & Sons Singapore Pte. Ltd. , 2014
3. M. Dusane and N.C. Ghuge., *A Review on Solar adsorption refrigeration systems*, IOSR Journal of Engineering. 2016
4. Wang, L.W., R.Z. Wang, R.G. Oliveira.. *A review on adsorption working pairs for refrigeration.* Renewable and Sustainable Energy Reviews,2009.
5. Wang, K., et al.. *Design and performance prediction of a novel double heat pipes type adsorption chiller for fishing boats*. Renewable Energy 2008.
6. Meunier, F., S.C. Kaushik, P. Neveu, and F. Poyelle. *Comparative thermodynamic study of sorption systems: second law analysis*. International Journal of Refrigeration.1996
7. EAV Kai, Wang PE, "New opportunities for solar adsorption refrigeration," ASHRAE Journal.,2011
8. R.Z. Wang, R.G. Oliveira, *Adsorption refrigeration-An efficient way to make good use of waste heat and solar energy*, Progress in Energy and Combustion Science. 2006
9. Wang X, Zimmermann W, Ng K, Chakraboty A, Keller J. *Investigation on the isotherm of silica gel+water systems.* Journal of Thermal Analysis and Calorimetry. 2004
10. Saha BB, Akisawa A, Kashiwagi T. *Solar/waste heat driven two-stage adsorption chiller*: *The prototype*. Renewable Energy. 2001
11. EAV Kai, Wang PE, *New opportunities for solar adsorption refrigeration*, ASHRAE Journal. September 2011
12. Gordeeva L, Grekova A, Krieger T, Aristov Y. *Binary salts in porous matrix for adsorption heat transformation*. Applied Thermal Engineering. 2013;**50**:1633-1638

13. Wang DC, Li YH, Li D, Xia YZ, Zhang JP. *A review on adsorption refrigeration technology and adsorption deterioration in physical adsorption systems*. Renewable and Sustainable Energy Reviews. 2010
14. Li H, Eddaoudi M, O'Keefe M, Yaghi OM. *Design and synthesis of an exceptionally stable and highly porous metal-organic framework*. Nature. Nov 1999
15. Mahmoud Salem Ahmed et al, *A Review: Future of the adsorption working pairs in cooling*, Sohag University. 2010
16. Meunier, F., Kaushik, S.C., Neveu, P. and Poyelle, F. *A comparative thermodynamic study of sorption systems: second law analysis*. International Journal of Refrigeration, 1996
17. Tchernev, D.I. and Emerson, D.T. *High-effciency regenerative zeolite heat pump.* ASHRAE, 1988
18. Shelton, S.V. (1990) Ramp wave analysis of the solid/vapor heat pump. *ASME Journal of Energy Resource Technology*,
19. Srivastava, N.C. and Eames, I.W. *A review of adsorbents and adsorbates in solid-vapour adsorption heat pump systems.* Applied Thermal Engineering, 1998
20. Miles, D. and Shelton, S. *Design and testing of a solid-sorption heat-pump system.* Applied Thermal Engineering, 1996.
21. Wang, L.W., Wu, J.Y., Wang, R.Z. et al., *Experimental study of a solidifed activated carbon-methanol adsorption ice maker.* Applied Thermal Engineering. 2003
22. Dunne, S., *Carousel heat exchanger for sorption cooling process*. US Patent 5 503 222. 1996
23. Pons, M. and Dantzer, P., *Heat transfer in hydride packed beds.* International Journal of Research in Physical Chemistry and Chemical Physics, 1994.
24. Vasiliev, L.L., *Heat pipes in modern heat exchangers*. Applied Thermal Engineering, 2005
25. Suzuki, M. *Application of adsorption cooling systems to automobiles*. Heat Recovery Systems and CHP. 1993

26. Zhu, R.Q., Han, B.Q., Lin, M.Z. and Yu, Y.Z. *Experimental investigation on an adsorption system for producing chilled water*. International Journal of Refrigeration, 1992.
27. Saha, B.B., Koyama, S., Ng, K.C. et al. *Study on a dual-mode, multi-stage, multi-bed regenerative adsorption chiller.* Renewable Energy, 2006.
28. Tchernev, D. Heat pump energized by low-grade heat sources. US Patent PCT/US85/00783. 1985.
29. Pons, M. and Guilleminot, J.J. *Design of an experimental solar-powered, solidadsorption ice maker*. ASME Journal of Solar Energy Engineering. 1986.
30. Grenier, P., Guilleminot, J.J. and Meunier, F., *Solar powered solid adsorption cold store.* Solar Energy Engineering. 1988
31. Sumathy, K. and Li, Z.F. (1999) Experiments with solar-powered adsorption ice maker. *Renewable Energy*,16, 704–707
32. Enibe, S.O. and Iloeje, O.C., *Transient analysis and performance prediction of a solid absorption solar refrigerator*. Solar Energy, 1997.
33. Vasiliev, L.L. *Heat pipes in modern heat exchangers*. Applied Thermal Engineering. 2005
34. Wai Soong Loh, Azhar Bin Ismail, Baojuan Xi, Kim Choon Ng, and Won Gee Chun. *Adsorption Isotherms and Isosteric Enthalpy of Adsorption for Assorted Refrigerants on Activated Carbons*. Journal of Chemical and Engineering Data. 2012
35. Ahmed A. Askalany, M. Salem, I.M. Ismail, Ahmed Hamza H. Ali, M.G. Morsy. *Experimental study on adsorption-desorption characteristics of granular activated carbon/R134a pair.* International journal of refrigeration 35(2012) 494-498. Elsevier
36. K Habib, M. Amin B. A. Majid, Shaharin Anwar B. Sulaiman. *Study on two stage activated carbon/HFC-134a based adsorption chiller*. IOP Conference Series: Earth and Environmental Science, 2013

37. N.D. Banker, M. Prasad, P. Dutta, K. Srinivasan. *Activated carbon + HFC 134a based two stage thermal compression adsorption refrigeration using low grade thermal energy sources.* Applied Thermal Engineering 29 (2009) 2257–2264
38. N.D. Banker[a,1], P. Dutta[a], M. Prasad[b], K. Srinivasan. *Performance studies on mechanical D adsorption hybrid compression refrigeration cycles with HFC 134a*. International journal of refrigeration 31(2008) 1398-1406
39. L.Z. Zhang, *Design and testing of an automobile waste heat adsorption cooling system*, Applied Thermal Engineerigg 20 (1) (2000) 103–114.
40. K.Habib, Khairul Habib, Bidyut Baran Saha, Shigeru Koyama. *Study of various adsorbent refrigerant pairs for the application of solar driven adsorption cooling in tropical climates.* Applied Thermal Engineering. ELSEVIER, 2014
41. Tamainot-Telto Z, Metcalf SJ, Critoph RE, Zhong Y, Thorpe R. *Carbon–ammonia pairs for adsorption refrigeration applications: ice making, air conditioning and heat pumping*. International Journal of Refrigeration, 2009
42. El-Sharkawy II, Hassan M, Saha BB, Koyama S, Nasr MM. *Study on adsorption of methanol onto carbon based adsorbents*. International Journal of Refrigeration. 2009

Appendix A: MATLAB code for performance analysis of activated carbon-R134a pairs

```
close all; clear all;
%%%%%%%%%%%%%%%%%%%%%%%%%%%%%%%%%%%%

A = 14.41; B = 2094; C = 33.06; %%Constants of Antoine equation
W_0 = [1.29, 1.68, 2.22]; %%Maximum adsorption capacities
W_1 = [1.4495, 1.3396, 1.2385, 1.0596, 0.9361]; %%Values of concentration for
isosteric heat of desorption
r1 = [1.49, 1.83, 1.29]; %%Constants of  of isosteric heat
r2 = [-0.001165, -0.000868, -0.001134]; %%Constants of D-A equation
T1 = [280, 285, 290, 300, 308]; %%Initial desorption temperature values
T2 = [304.719, 310.277, 315.83, 326.934, 335.81]; %%Temperature values at the
end of isosteric heating
Cpa = 0.9; Cpr = 1.43; Cps = 0.434; %%Specific heat capacities of activated
carbon and R-134a
Qrad = [183.86 184.375 173.926 138.06 158.896 123.107 134.323 133.084 176.613
184.635 180.257 192.073];%%Radiation values from Metrology
hfg = 209.5; %%Latent heat of vaporization of R134a (kJ/kg.K)
ma = 1; %%mass of activated carbon
mf = 0.037; map = 0.0465; mb = 3.82;
Wa = 1.4495;
Ta = 280;
Tb = 304.719;
Tg1 = 353;
Wa1 = 1.0979;
Ta1 = 280;
Tb1 = 304.719;
%%% Intialize %%%%

Tgen = 338:1:363;
Ps = exp(A - (B./(Tgen-C))); %%Saturation pressure calculation (kPa)
t = 1:0.1:5.4;
t2 = 5.4:-0.1:1;
m = 1;

for n = 3
    for k = 1:length(W_1)
    Wmin= (W_0(n).*((Ps./600.023).^(r1(n).*r2(n).*Tgen))); %%adsorption
capacity at the end of desorption
    mr134 = ma.*(W_1(k) - Wmin); %%Calculation of Total mass of R134a
desorbed
    Q12 = ((ma.*Cpa) + (mr134.*Cpr))*(T2(k) - T1(k))+(mf.*Cps)*(T2(k)-T1(k))
+ (map.*Cps)*(T2(k)-T1(k)) + (mb.*Cps)*(T2(k)-T1(k)); %%Calculation of heat
applied during isosteric heating
    H = 8.314.*C.*(Tgen./T2(k));
    Q23 = (ma.*Cpa + Cpr.*(W_1(k) + Wmin)./2).*(Tgen-T2(k))+ ((ma.*(W_1(k) -
Wmin)).*H) + (mf.*Cps)*(Tgen-T2(k))+ (mb.*Cps)*(Tgen-T2(k))+(map.*Cps)*(Tgen-
T2(k)); %%Calculation of heat applied during isobaric desorption
    Qe = (W_1(k)-Wmin).*hfg; %% cooling capacity of evaporator
    cop_cyc = Qe./(Q12+Q23); %%cycle COP calculation
    scp = (((W_1(k)-Wmin).*hfg + (Cpr.*(W_1(k) - Wmin)).*(Tgen-
T1(k))./(5.4)); %%Specific cooling power calculation
```

```
    figure(m)
    plot(Tgen,cop_cyc); %%Plot of cycle COP versus generation temperature
    xlabel('Generation temperature(K)'); ylabel('Cycle COP');
    legend
('280K','285K','290K','300K','308K','location','eastoutside','orientation','v
ertical')
    hold on
    figure(m+1)
    plot(Wmin,cop_cyc); %%plot of cycle COP versus adsorption capacity at the
end of desorption
    xlabel('Final Desorbed concentration(kg/kg)'); ylabel('Cycle COP');
    legend
('280K','285K','290K','300K','308K','location','eastoutside','orientation','v
ertical')
    hold on
    figure(m+3)
    plot(Tgen,scp); %% plot of SCP versus generation temperature
    xlabel('Generation temperature(K)'); ylabel('SCP (W/kg)');
    legend
('280K','285K','290K','300K','308K','location','eastoutside','orientation','v
ertical')
    hold on
    figure(m+4)
    plot(scp,cop_cyc);%% plot of SCP versus cycle COP
    xlabel('SCP (W/kg)'); ylabel('Cycle COP (kg/kg)');
     legend
('280K','285K','290K','300K','308K','location','eastoutside','orientation','v
ertical')
    hold on

      end
end

%%Optimization of the generation temperature
    for l = 1:length(Tgen)
      Pss = exp(A - (B./(Tgen(l)-C)));
      Wm(l)= (1.68.*((Pss./600.023).^((-0.00158844).*Tgen(l))));
      scp2(l)= ((((Wa-Wm(l)).*hfg) + ((Cpr.*(Wa - Wm(l))).*(Tgen(l)-
Ta))./(5.4));
      mr134a = ma.*(Wa - Wm(l));
      Qa = ((ma.*Cpa) + (mr134a.*Cpr))*(Tb-Ta)+(mf.*Cps)*(Tb-Ta) +
(map.*Cps)*(Tb-Ta) + (mb.*Cps)*(Tb-Ta);
      Qx1(l) = (Wa-Wm(l)).*hfg;
      Hb1(l) = 8.314.*C.*(Tgen(l)./Tb);
      Qb(l) = (ma.*Cpa + Cpr.*(Wa + Wm(l))./2).*(Tgen(l)-Tb)+ ((ma.*(Wa -
Wm(l))).*Hb1(l)) + (mf.*Cps)*(Tgen(l)-Tb)+ (mb.*Cps)*(Tgen(l)-
Tb)+(map.*Cps)*(Tgen(l)-Tb);
      cop2(l) = (Qx1(l))./(Qa+Qb(l));
    end
 figure(m+2);
 plotyy(Tgen,scp2,Tgen,cop2)
grid on
```

```
 %%m = m+6;
    figure(m+5)
     plot3(Tgen,Wmin,cop_cyc);
    xlabel('Generation temperature'); ylabel('Wminimum'); zlabel('Cycle
COP');
    hold on
      figure(m+6)
    for j = 1:12
        for d = 1:length(Qe)
    cop_rad(j) = Qe(d)./(Qrad(j).*(5.4));
    plot(cop_rad); %%plot of monthly solar COP
    xlabel('Month'); ylabel('Solar COP');
    hold on
        end
    end

    hold off
```

Appendix B: MATLAB code for plotting cycle diagrams of activated carbon-R134a pairs

```
close all; clear all;
%--Constants--%
A = 14.41;  B = 2094; C = 33.06;

W_0 =
2.2;
r1 = 1.29;  %% D-A equation constant (vary this value for other AC types)
r2 = -0.001134; %% D-A equation constant (vary this value for other AC
types)
T = 253:5:373; P = 1:10:1000;
 W1 = 0.1:0.1:2.2; %% D-A equation constant (vary this value for other AC
types)
P_s = A - (B./(T-C));
P_s1 = exp(P_s);

  for m = 1:length(W1)
for k = 1 : length(T)
        P2(k,m)
=(P_s1(k))./((W1(m)./W_0)^(1/(r1*r2*T(k))));          end
end

%%% Plots %%%%%%%%%%%%%%%

W_1 = 1.2955;
W_2 = 1.1085;
Pcond = 599.99;
Pev = 270;
```

```
%%%%First equation of
cycle% m = 1; n=1; i=1;
j=1; for Td = 308:0.2:348

    if Td<=335.81
        Pd = exp(A - (B./(Td-C)));
P1(m)= Pd/(W_1/W_0)^(1/(r1*r2*Td));
m = m+1;     end
    if Td>=335.81 &&
Td<=348          P_2(n) =
Pcond;          n = n+1;
end     if Td>=319 &&
Td<=348
        Pd = exp(A - (B./(Td-C)));
P3(i)= Pd/(W_2/W_0)^(1/(r1*r2*Td));
i = i+1;     end     if Td>=308 &&
Td<=319          P4(j) = Pev;          j
= j+1;            end

end
%Plots figure(4) for m = 1:length(W1)
semilogy(T,P2(:,m)); %%plot of p-T-w
diagram hold on end hold on

Td=308:0.2:335.81;
semilogy(Td,P1,'k-', 'LineWidth', 1); %%plot of cycle
diagram hold on Td=335.81:0.2:348;
semilogy(Td,P_2,'k-', 'LineWidth', 1); %%plot of cycle
diagram hold on  Td=319:0.2:348;
semilogy(Td,P3,'k-', 'LineWidth', 1); %%plot of cycle diagram hold on
Td = 308:0.2:319;
semilogy(Td,P4,'k-', 'LineWidth', 1); %%plot of cycle diagram hold off
title('Maxsorb III')
legend('0.1','0.2','0.3','0.4','0.5','0.6','0.7','0.8','0.9','1','1.1','1.
2',
'1.3','1.4','1.5','1.6','1.7','1.8','1.9','2','2.1','2.2','location','east
out side','orientation','vertical')
xlabel('T (K)'); ylabel('P (kPa)');
```

Appendix C: MATLAB code for plotting Adsorption isotherm and p-T-W diagrams of activated carbon-R134a pairs

```
%%%%%%%%%%%%%%%%%%%%%%%%%%%%%%%%%%%%%%%%%%%%%%%%%%%%%%%%%%%%%%%%%%%%%%%%%%%%
Close all; clear all;
%--Constants--%
A = 14.41;
B = 2094;
C = 33.06;

W_0 = [1.29, 1.68, 2.22]; %maximum concentration (adsorption capacities)
```

```
Tc = 20:10:90; Tc1 = Tc+273.15; % in K r1 = [1.49, 1.83, 1.29]; %
exponential constant values of D-A equations  r2 = [-0.001165, -
0.000868, -0.001134]; %constant values of D-A equations
T = 253:5:373;
P = 1:10:1000;
%%% Saturation Temprature %%%%%%%%%%%%%%%%%%%%%%%%%%%%%%%%%%%%%%%%%%%%%%%%
P_s = A - (B./(Tc1-C)); %% saturation pressure calculation
P_s1 = exp(P_s);   %P_s1 was used in the D-A equation instead of
P_s
%--------------- Figure 1 ---------------------------------
%%%%%%%%%%%%%%% for n = 1:3
  for m = 1:length(Tc1)
for k = 1 : length(P)
if P(k)<=P_s1(m)
        W(k,n,m)=
(W_0(n).*((P_s1(m)./P(k)).^(r1(n).*r2(n).*Tc1(m))));
end         end   end end
%Plots
figure(
1)
for m = 1:length(Tc1)
in =
find(W(:,1,m)>0);
plot(P(1:in(end)),W(1:in(end),1,m)); %%plot of pressure versus
adsorption capacity for ACF-A20-R134a pairs hold on end hold off
title('ACF-A20')
legend('293.15K','303.15K','313.15K','323.15K','333.15K','343.15K','35
3.15K',
'363.15K','Location','eastoutside','orientation','vertical');
xlabel('P (kPa)'); ylabel('W (kg/kg)');
    figure(2) for
m = 1:length(Tc1)
in =
find(W(:,2,m)>0);
plot(P(1:in(end)),W(1:in(end),2,m));%%plot of pressure versus adsorption
capacity for Granular AC-R134a pairs hold on end hold off title('Granular
AC')
legend('293.15K','303.15K','313.15K','323.15K','333.15K','343.15K','353.15
K',
'363.15K','Location','eastoutside','orientation','vertical');
xlabel('P (kPa)'); ylabel('W (kg/kg)');
 figure(3) for m =
1:length(Tc1) in =
find(W(:,3,m)>0);
plot(P(1:in(end)),W(1:in(end),3,m));%%plot of pressure versus adsorption
capacity for Maxsorb III-R134a pairs hold on end hold off title('Maxsorb-
III')
legend('293.15K','303.15K','313.15K','323.15K','333.15K','343.15K','353.15
K',
'363.15K','Location','eastoutside','orientation','vertical');
xlabel('P (kPa)'); ylabel('W (kg/kg)');
```

```
%--------------- Figure 2 ---------------------------------%%%%%%%%%%%%%%%
%%%%%%%%%%%%%%%%%%%% p-T-W diagrams %%%%%%%%%%%%%%%%%%%%%%%%%%%%%%%

W1 = 0.1:0.1:1.29;
W2 = 0.1:0.1:1.68;
W3 = 0.1:0.1:2.22;

P_s = A - (B./(T-C));
P_s1 = exp(P_s);

       for m =
1:length(W1)
           for k = 1 :
length(T)
        P2(k,1,m) =(P_s1(k))./((W1(m)./W_0(1))^(1/(r1(1).*r2(1).*T(k))));

%%(P_s1(k))./((W1(m)./W_0)^(1/(r1*r2*T(k))))
end     end %Granular AC for m = 1:length(W2)
         for k = 1 :
length(T)
        P2(k,2,m) =(P_s1(k))./((W2(m)./W_0(2))^(1/(r1(2).*r2(2).*T(k))));
end
end

%Maxsorb-III for m =
1:length(W3)     for k
= 1 : length(T)
        P2(k,3,m)
=(P_s1(k))./((W3(m)./W_0(3))^(1/(r1(3).*r2(3).*T(k))));       end
end

%%% Plots %%%%%%%%%%%%%%%

%Plots
figure(
4)
for m = 1:length(W1) semilogy(T,P2(:,1,m)); %%plot of p-T-w diagram
for ACF-A20-R134a pairs hold on end hold off title('ACF-A20')
legend('0.1','0.2','0.3','0.4','0.5','0.6','0.7','0.8','0.9','1','1.1','1.
2',
'Location','eastoutside','Orientation','vertical')
xlabel('T (K)'); ylabel('P (kPa)');

figure(
5)
for m = 1:length(W2) semilogy(T,P2(:,2,m));%%plot of p-T-w diagram for
Granular AC-R134a pairs hold on end hold off;
legend('0.1','0.2','0.3','0.4','0.5','0.6','0.7','0.8','0.9','1','1.1','1.
2',
'1.3','1.4','1.5','1.6','Location','eastoutside','Orientation','vertical')
title('Granular') xlabel('T (K)'); ylabel('P (kPa)');
```

```
figure
(6)
for m = 1:length(W3) semilogy(T,P2(:,3,m)); %%plot of p-T-w diagram for
MAxsorb III-R134a pairs hold on end hold off; title('Maxsorb-III')
legend('0.1','0.2','0.3','0.4','0.5','0.6','0.7','0.8','0.9','1','1.1','1.
2',
'1.3','1.4','1.5','1.6','1.7','1.8','1.9','2','2.1','2.2','Location','east
out side','Orientation','vertical')
xlabel('T (K)'); ylabel('P (kPa)');
```

Appendix D: Solar Radiation Data for the year 2018

Month of Year	**Average Monthly solar Radiation (W/m^2)**
January	183.8645161
February	184.375
March	173.9258065
April	138.06
May	158.8967742
June	123.107
July	134.3225806
August	133.083871
September	176.6133333
October	184.6354839
November	180.2566667
December	192.0733333